Review of Scientific Instruments

A review of design approaches for the implementation of low-frequency noise measurement systems

Cite as: Rev. Sci. Instrum. **93**, 111101 (2022); https://doi.org/10.1063/5.0116589
Submitted: 29 July 2022 • Accepted: 20 October 2022 • Published Online: 21 November 2022

G. Scandurra, C. Ciofi, J. Smulko, et al.

COLLECTIONS

EP This paper was selected as an Editor's Pick

View Online Export Citation CrossMark

Fast, Sensitive and Reliable Leak Detection: ASM 340
PFEIFFER VACUUM

© 2022 Author(s).

A review of design approaches for the implementation of low-frequency noise measurement systems

Cite as: Rev. Sci. Instrum. 93, 111101 (2022); doi: 10.1063/5.0116589
Submitted: 29 July 2022 • Accepted: 20 October 2022 •
Published Online: 21 November 2022

View Online

Export Citation

CrossMark

G. Scandurra,[1,a)] C. Ciofi,[1] J. Smulko,[2] and H. Wen[3]

AFFILIATIONS

[1] Department of Engineering, University of Messina, Messina 98166, Italy
[2] Department of Metrology and Optoelectronics, Gdańsk University of Technology, 80-233 Gdańsk, Poland
[3] College of Electrical and Information Engineering, Hunan University, Changsha 410082, China

[a)] Author to whom correspondence should be addressed: gscandurra@unime.it

ABSTRACT

Electronic noise has its roots in the fundamental physical interactions between matter and charged particles, carrying information about the phenomena that occur at the microscopic level. Therefore, Low-Frequency Noise Measurements (LFNM) are a well-established technique for the characterization of electron devices and materials and, compared to other techniques, they offer the advantage of being non-destructive and of providing a more detailed view of what happens in the matter during the manifestation of physical or chemical phenomena. For this reason, LFNM acquire particular importance in the modern technological era in which the introduction of new advanced materials requires in-depth and thorough characterization of the conduction phenomena. LFNM also find application in the field of sensors, as they allow to obtain more selective sensing systems even starting from conventional sensors. Performing meaningful noise measurements, however, requires that the background noise introduced by the measurement chain be much smaller than the noise to be detected and the instrumentation available on the market does not always meet the specifications required for reaching the ultimate sensitivity. Researchers willing to perform LFNM must often resort to the design of dedicated instrumentation in their own laboratories, but their cultural background does not necessarily include the ability to design, build, and test dedicated low noise instrumentation. In this review, we have tried to provide as much theoretical and practical guidelines as possible, so that even researchers with a limited background in electronic engineering can find useful information in developing or customizing low noise instrumentation.

Published under an exclusive license by AIP Publishing. https://doi.org/10.1063/5.0116589

I. INTRODUCTION AND HISTORICAL OVERVIEW

Low-Frequency Noise Measurement (LFNM) technique has been used as a tool for the characterization of the quality and reliability of electron devices since the latest 1940s when investigation on the low-frequency noise in thermionic valves under amplifying conditions began to be conducted.[1] Since then, the LFNM technique has accompanied the technological progress in the field of electronic devices and materials, so much so that the results of the search for the terms "low-frequency noise" on the Scopus database are the mirror of the evolution in the field. In the publications of the 1950s, there are studies on noise in electron tubes[2–4] and the interest on the characterization of Germanium is evident, mainly for its importance, at that time, in the understanding of diode and transistor technology.[5,6] In 1950, we have the first publication (according to the research carried out in the Scopus Database) in which the problem of noise in (valve) amplifiers for applications in the biological field is addressed.[7] In the 1960s, there are several characterization works, by means of noise measurements, of diodes[8–12] and, since the end of the 1960s, the scientific literature has been enriched with numerous works dedicated to the study of field-effect transistor (FET) transistors on the basis of noise measurements.[13–16] In the 1970s, scientific publications[17–30] testify to a considerable commitment to the physical interpretation of the origins of noise in devices, and the results obtained are used to improve the steps of technological processes required for the manufacture of the devices themselves. Since the 1980s, with the emergence of VLSI technology, noise measurements have become a very effective tool for the characterization of

MOST WIEDZY Downloaded from mostwiedzy.pl

interconnections in integrated circuits. In fact, LFNM is a performant technique for the characterization of electromigration of metal interconnections in that the evaluation of the activation energy can be performed at less severe test conditions than those characteristics of other techniques.[31,32] This application has continued steadily over the years,[33–38] up to the present day, where it is widely used for the characterization of advanced interconnects,[39–42] which, given the need for particular test conditions (with reference to temperature), in some cases may require the use of custom-made instrumentation.[42] In addition to electromigration, in the years of affirmation of VLSI technology, there was another main problem concerning the reliability of integrated circuits: the electrical breakdown of thin silicon dioxide layers. The analysis of the low-frequency fluctuations of the current tunneling through the thin oxide layer showed that it was possible to interrupt stress tests just a few seconds before the occurrence of the destructive breakdown phase, which typically results in such severe damage that no meaning failure analysis can be carried afterward. This important difference with more conventional reliability characterization techniques, in which the complete destruction of the device cannot be avoided, has resulted in an invaluable help in understanding specific aspects of the failure mechanisms in field effect devices.[43–47] Over the years, LFNMs have been applied to the characterization of all electronic devices being introduced, up to the most current times, where they play an important role in the understanding of the conduction mechanisms in advanced devices, such as organic transistors,[48–54] 2D materials and devices,[55–59] solar cells,[60–71] photodetectors,[72–81] and sensors.[82–94] Quite remarkably, in the case of chemical sensors, the fact that LFNM carries information about the detailed interaction of the carrier with the sensor matrix can be exploited for enhancing the sensitivity of the sensor with the ability to distinguish between different analytes on the basis of the detailed features in the measured spectra.[95]

Despite the advantages and the different possibilities of the application of LFNM, performing meaningful noise measurements is never an easy task since it is required that the background noise introduced by the measurement chain be much smaller than the noise to be detected. The instrumentation available on the market does not always meet the specifications required for reaching the ultimate sensitivity that would be required in many interesting instances. For this reason, researchers willing to perform LFNM with high sensitivity must resort to the design of dedicated instrumentation in their own laboratories. However, not all the researchers interested in performing noise measurements possess the necessary skills, often having a cultural background more in the field of physics or chemistry rather than electronic instrumentation. This is the reason that led us to collect, in this review paper, the main theoretical knowledge, the measurement techniques, and set-ups that can act as a reference for those wishing to undertake LFNM characterizations. This paper is organized as follows: in Sec. II, noise estimation techniques are outlined; in Secs. III and IV, the most appropriate measurement solutions will be illustrated based on the impedance value of the Device Under Test (DUT); in Sec. V, applications of LFNM on sensors are reported; in Sec. VI, the issue of 2D materials' characterization is considered; in Sec. VII conclusions are drawn.

II. NOISE ESTIMATION TECHNIQUES

A. Circuit configurations

In order to simplify the discussion, we will restrict ourselves to the case of the measurement of noise on two pole devices. This is not as limiting as it might appear at first sight, since in many cases of interest measurement on active devices can be thought of as performed on one single port while the other port is maintained at a fixed bias. It is worth noticing that noise measurements on a device are necessarily performed with the device being part of a circuit containing other active and passive components. This is schematically shown in Fig. 1(a), where the DUT represents the device whose noise properties are being investigated. In a circuit like the one in Fig. 1(a), we can, at best, detect and analyze the voltage fluctuations v_n across the device, ideally by means of a noiseless voltage amplifier with infinite input impedance and gain A_V, or we can modify the circuit as in Fig. 1(b) by introducing an ideal transimpedance amplifier with gain A_R to detect and analyze the fluctuations of the current i_n flowing through the DUT. Clearly, the fluctuations of both the voltage v_n and the current i_n [and the corresponding Power Spectral Densities (PSD) S_{vn} and S_{in}] cannot be attributed to the DUT alone but are the result of the contribution of all noise sources present in the circuit. Moreover, even in the hypothetical case of the DUT being the only source of fluctuations, v_n and i_n change as the circuit to which the DUT is connected changes. When we investigate the noise generated by a DUT in the context of LFNM, we make reference to either one of the two equivalent representations in Fig. 2, where Z_D is the small signal equivalent impedance at any given DC bias. In particular, we can quantify the noise generated by a specific device either in terms of the PSD S_{vD} of an ideal equivalent internal voltage noise source v_{Dn} in series with Z_D [Fig. 2(a)], or in terms of the PSD S_{iD} of an ideal internal equivalent current source i_{Dn} in parallel with Z_D [Fig. 2(b)].

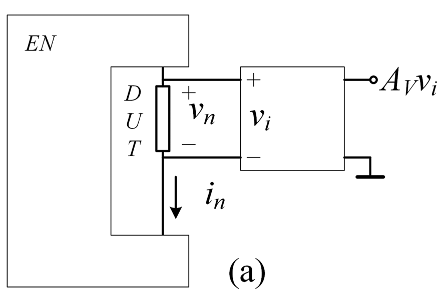

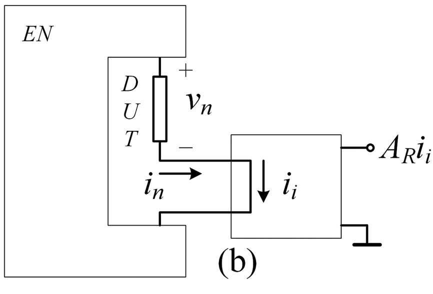

FIG. 1. Voltage (a) and current (b) noise measurements in a DUT that is part of an Electronic Network (*EN*). The noise signals v_n and i_n are, in the general case, the result of the noise contributions coming from the DUT and from the other noise sources present in the network.

ublished under an exclusive license by AIP Publishing

MOST WIEDZY Downloaded from mostwiedzy.pl

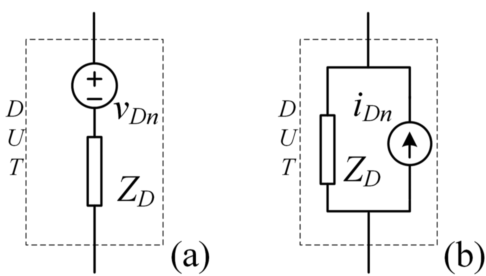

FIG. 2. Two equivalent representations of a DUT generating noise. In (a), the noise is represented by a voltage source in series with the impedance, and in (b), the noise source is represented with a current source in parallel with the impedance.

For the two representations to be equivalent, it is required that

$$S_{vD} = |Z_D|^2 S_{iD}. \quad (1)$$

Equation (1), which descends from general principles,[96] tells us that, as long as Z_D is known, we can obtain S_{vD} from the knowledge of S_{iD} and vice versa. The problem is that, while we are interested in S_{vD} (or, equivalently in S_{iD}), we have only access, from an experimental point of view, to either S_{vn} [Fig. 1(a)] or to S_{in} [Fig. 1(b)]. Therefore, consequently what we need to employ a circuit configuration, for the *EN* in Fig. 1, that makes it possible to obtain either S_{vD} or S_{iD} (that cannot be directly measured) from S_{vn} or S_{in} (that can be estimated experimentally). Let us assume that we deal with a DUT to be biased at a DC voltage V_D. Let I_D and Z_D be the DC and the small signal impedance, respectively, corresponding to the bias voltage V_D. Figure 3(a) shows a quite common circuit configuration that is used to bias a DUT, with V_B and R_B selected in such a way as to obtain the desired DC voltage V_D across the DUT, according to the solution of the following system:

$$\begin{cases} I_D = \dfrac{V_B - V_D}{R_B}, \\ I_D = f_D(V_D), \end{cases} \quad (2)$$

where $f_D(V_D)$ is the current–voltage characteristic of the DUT. If we assume no restriction in the values of V_B and R_B, there are infinite values of V_B and R_B for which we can obtain the same operating point I_D-V_D for the DUT.

This observation becomes important when we look at the equivalent circuit for noise calculation in Fig. 3(b). Assuming that we employ excess noise-free resistors for R_B, the bias resistance introduces thermal noise only. If we further assume all noise sources to be uncorrelated, we have, for the PSD S_{vn} of the voltage v_n across the DUT,

$$S_{vn} = (S_{vnB} + 4kTR_B)\left|\frac{Z_D}{Z_D + R_B}\right|^2 + S_{vD}\left|\frac{R_B}{Z_D + R_B}\right|^2, \quad (3)$$

where k is the Boltzmann constant, T is the absolute temperature, and S_{vnB} is the PSD of the voltage fluctuations introduced by the bias voltage. In the same way, and using Eq. (1), we can estimate the PSD S_{in} of the current fluctuations i_n through the DUT as follows:

$$S_{in} = \frac{S_{vnB} + 4kTR_B}{|Z_D + R_B|^2} + S_{iD}\left|\frac{Z_D}{Z_D + R_B}\right|^2. \quad (4)$$

As it is apparent from Eqs. (3) and (4), S_{vn} and S_{in} do not coincide with either S_{vD} or S_{iD}, respectively. However, let us assume that we can increase both V_B and R_B while obtaining the same bias point for the DUT. Let us also assume, as it is often the case, that the noise introduced by the bias voltage is much smaller than the noise introduced by the resistance R_B for increasing R_B. With these assumptions, for sufficiently large values of R_B ($R_B \gg |Z_D|$), S_{vn} becomes essentially coincident with S_{vD}, and therefore, in these conditions, S_{vn} can provide a quite good estimate of S_{vD}. On the other hand, if we go in the opposite direction, for very small values of R_B with respect to $|Z_D|$, from Eq. (4) we obtain that, provided the contribution S_{vnB} is negligible, S_{in} essentially reduces to S_{iD}. From these observations, it would appear that, at least in principle, we can always bias the DUT in either one of the limiting conditions so that we can perform either direct measurement of the PSD of the internal voltage noise of the DUT or direct measurement of the internal current noise of the DUT. However, when we work with a relatively high value for the impedance Z_D, it might be impractical to reach the necessary condition $R_B \gg |Z_D|$, not to mention the fact that also the corresponding values for V_B required to reach a specified bias point might become prohibitively large. In these case, therefore, it is generally better to work in the other limiting condition, that is the one in which we can obtain a direct estimation of S_{iD} with $R_B = 0$ and $V_B = V_D$; on the other hand, when working with relatively small values for Z_D, it might not be possible to neglect the contribution from the noise introduced by the bias voltage as it can be easily deduced from Eq. (4). In these cases, therefore, the best approach is that of working in the conditions in which a direct estimate of the voltage noise can be obtained (i.e., large values of V_B and R_B). Clearly, there is no general way to define an impedance

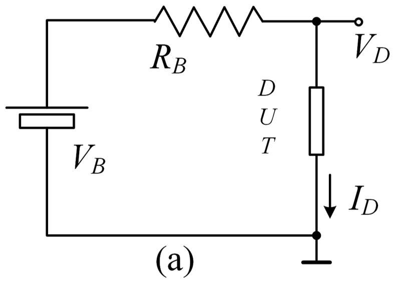

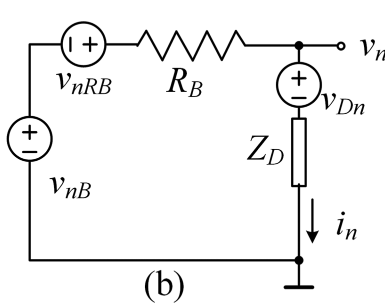

FIG. 3. Actual circuit configuration for biasing the DUT and performing noise measurements (a); the small signal equivalent circuit in (b) is used for noise calculation.

MOST WIEDZY Downloaded from mostwiedzy.pl

ublished under an exclusive license by AIP Publishing

value below which is always convenient to perform voltage noise measurements, and above which it is always convenient to perform current noise measurements. Several factors may contribute to this choice, and among these factors, the additional noise that is introduced by the amplifiers (either voltage amplifiers or transimpedance amplifiers, depending on the measurement configuration) plays an important role, as will be discussed later in the paper. It is however not a case that when LFNM is employed in the investigation of electromigration, where samples have impedances that are typically in the hundreds of ohms, voltage noise measurements are preferred, while in the case of the investigation of thin oxides, with extremely high impedance at low frequencies, current noise measurements are used for the characterization of their noise.

Whatever configuration is used for detecting the noise generated by the DUT, a low noise amplifier is used (either a voltage amplifier or a transimpedance amplifier) to raise the level of the signal so that it can be more easily elaborated for extracting an estimate of the noise PSD.

B. A brief summary of power spectral estimation using the discrete Fourier transform

From an experimental point of view, PSD estimation relies on the assumption of ergodicity for the process being investigated since, in general, we have only one single realization of the process available.[97] Suppose that, as illustrated in Fig. 4, the noise signal $v_s(t)$, with a bilateral PSD $S_B(f)$, is fed to the input of an ideal band-pass filter centered at f_k and with a bandwidth Δf, that is with a bilateral frequency response $H_B(f)$,

$$H_B(f) = \begin{cases} 1 & \textit{if} \quad |f \pm f_k| < \dfrac{\Delta f}{2}, \\ 0 & \textit{otherwise} \end{cases} \tag{5}$$

then, for the bilateral PSD $S_{Bk}(f)$ of the signal $v_{sk}(t)$ at the output of the filter, we can write

$$P_{Bk} = \int_{-\infty}^{+\infty} S_{Bk}(f)df = \lim_{\Delta T \to \infty} \frac{1}{\Delta T} \int_{-\Delta T/2}^{+\Delta T/2} v_{sk}^2(t)dt, \tag{6}$$

where P_{Bk} is the power of the process $v_{sk}(t)$. If we can select Δf sufficiently small so that we can assume $S_B(f)$ to be constant and almost equal to $S_B(f_k)$ within the bandwidth of the filter, we have, for the left-hand side in Eq. (6),

$$\int_{-\infty}^{+\infty} S_{Bk}(f)df = \int_{-f_k-\frac{\Delta f}{2}}^{-f_k+\frac{\Delta f}{2}} S_B(f)df + \int_{+f_k-\frac{\Delta f}{2}}^{+f_k+\frac{\Delta f}{2}} S_B(f)df$$
$$\approx [S_B(-f_k) + S_B(f_k)]\Delta f = 2S_B(f_k)\Delta f. \tag{7}$$

We have used the fact that the bilateral PSD $S_B(f)$ of the real noise signal $v_s(t)$ is an even function of the frequency.

As far as the right-hand side of Eq. (6) is concerned, in actual measurements, we can neither go back in time nor we can wait forever to obtain an estimate, and therefore the assumption is made that, using also Eq. (7), we can rewrite Eq. (6) as follows:

$$\int_{-\infty}^{+\infty} S_{Bk}(f)df = 2S_B(f_k)\Delta f$$
$$\approx \frac{1}{T}\int_0^T v_{sk}^2(t)dt \quad \text{for a sufficiently large } T. \tag{8}$$

The amount of time T required to reach a good estimate of the power spectral density is a key parameter to be taken into consideration when planning and performing actual noise measurements and we need to discuss this aspect. In order to obtain the PSD at a given frequency f_k, we can follow an approach that is essentially equivalent to the one discussed so far and that it is much closer to the actual approach that is used in modern dynamic signal analyzers. This second approach is schematically depicted in Fig. 5. Note that in this case the output of the low-pass filter is a complex signal and that we can select different frequencies at which to perform the estimation of the spectrum by changing the frequency f_k of the

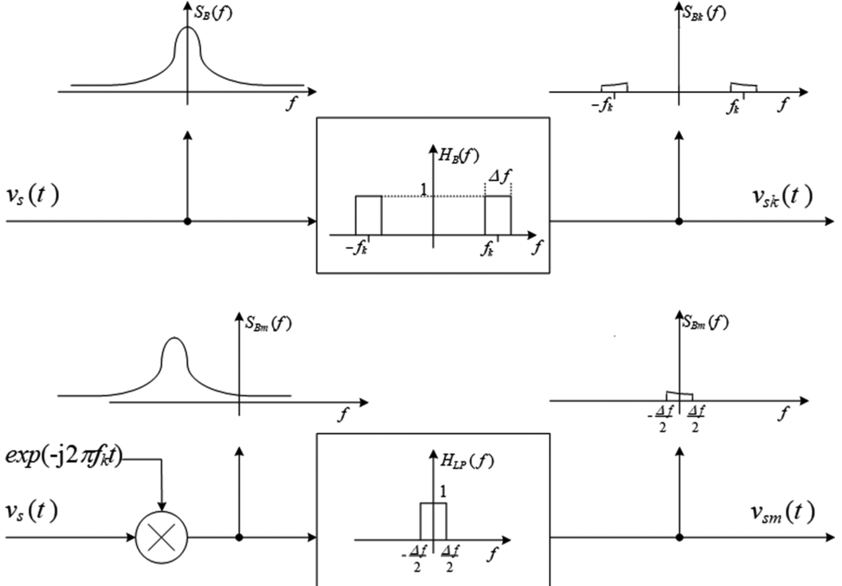

FIG. 4. Ideal signal processing in the continuous time domain for filtering out the PSD of the input process at all frequency but in a small frequency bandwidth Δf across f_k.

FIG. 5. Ideal signal processing in the continuous time domain for selecting the PSD in a small frequency interval across f_k by resorting to frequency translation and low pass filtering. The sample and hold circuit at the output is used to obtain the value of the process at the output of the system at discrete time intervals.

MOST WIEDZY Downloaded from mostwiedzy.pl

complex exponential signal that causes a translation of the PSD. We have, for the PSD $S_{Bm}(f)$ at the output of the multiplier,

$$S_{Bm}(f) = S_B(f - f_k). \tag{9}$$

With the same argument as before, provided that $S_{Bm}(f)$ does not change much within the bandwidth of the low pass filter, we have

$$\int_{-\infty}^{+\infty} S_{Bm}(f)df = \int_{-\frac{\Delta f}{2}}^{+\frac{\Delta f}{2}} S_{Bm}(f)df = \int_{+f_k-\frac{\Delta f}{2}}^{+f_k+\frac{\Delta f}{2}} S_B(f)df = S_B(f_k)\Delta f. \tag{10}$$

Equation (8), in the case at hand, becomes

$$S_B(f_k)\Delta \mathrm{f} = \frac{1}{T}\int_0^T |v_{sm}(t)|^2 dt \quad \text{for a sufficiently large } T, \tag{11}$$

where v_{sm}(t) is the complex signal at the output of the low pass filters with bandwidth $\Delta f/2$ in Fig. 5.

In order to obtain an estimate of the averaging time that is required for obtaining a good estimate of $S_B(f_k)$ from the integration, let us assume, for the sake of simplicity, that $S_B(f_k)$ is exactly constant within the bandwidth of the filter. Let S_{BT} be the stochastic variable that represent the estimate of $S_B(f_k)$ over an integration time T according to the right-hand side of Eq. (11), that is,

$$S_{BT}(f_k) = \frac{1}{T\Delta f}\int_0^T |v_{sm}(t)|^2 dt. \tag{12}$$

We are interested in the estimate of the average η_{SBT} and of the standard deviation σ_{SBT} as a function of T. Clearly, we have

$$\begin{aligned}\eta_{SBT} = E[S_{BT}] &= \frac{1}{T\Delta f}\int_0^T E\left[|v_{sm}(t)|^2\right]dt \\ &= \frac{1}{T\Delta f}\int_0^T S_B(f_k)\Delta f dt = S_B(f_k).\end{aligned} \tag{13}$$

As far as the standard deviation is concerned, which is a measure of the uncertainty in the estimate, following the procedure outlined in Davenport *et al.*[98] and in Bennet and Fulton,[99] we obtain that for very low values of T, which essentially corresponds to sampling a single value of $v_{sm}(t)$, and taking its squared modulus as an estimate of the power at the output of the low-pass filter, we have

$$\sigma_{SBT} = \sqrt{E\left[S_{BT}^2\right] - \eta_{SBT}^2} = S_B(f_k), \tag{14}$$

and this means that the standard deviation of the error is equal to the quantity to be estimated. However, for large values of T (with respect to the inverse of the bandwidth of the filter[98]), we have

$$\sigma_{SBT} = \sqrt{E\left[S_{BT}^2\right] - \eta_{SBT}^2} = \frac{S_B(f_k)}{\sqrt{2T\Delta f}} \Rightarrow \varepsilon_r = \frac{\sigma_{SBT}}{S_B(f_k)} = \frac{1}{\sqrt{2T\Delta f}}. \tag{15}$$

The result in Eq. (15) is extremely important in the field of low frequency noise measurements. Even without taking into account the fact that we do not have an ideal low-pass filter available, it sets a fundamental relationship among the accuracy that we hope to obtain (ε_r), the bandwidth that we employ to select a portion of the PSD to be estimated and the time required for obtaining such estimate. As we shall see in a moment, modern signal analyzers can perform spectral estimation in parallel on many frequencies at the same time, but because of the fact that the PSD of flicker noise is inversely proportional to the frequency, exploring lower and lower frequencies requires smaller and smaller values of Δf. If the minimum frequency of interest is f_{min}, Δf should be much smaller in order to ensure that we can assume the spectrum constant in a bandwidth Δf across f_{min}. If we assume that we are interested in f_{min} = 100 mHz, and therefore select Δf = 10 mHz, and we would like to obtain a relative error of less than 5% (ε_r = 0.05) in the estimate of the spectrum, from Eq. (15), we obtain that the required measurement time is in excess of 24 h. This simple example demonstrates that the ability to correctly balance the requirements in terms of accuracy, minimum frequency of interest, and measurement time is one of the key aspects that need to be addressed when performing low-frequency noise measurements.

In the class of spectral analyzers we are interested in, the estimation of the PSD is generally performed in the numeric domain, starting from a sampled version of the input signal, exploiting the modified periodogram approach developed by Welch in 1967.[100] Rather than following a rigorous approach in the domain of stochastic sequences, in this review, we would like to follow a different avenue that allows us to obtain the relationships that are actually employed in spectrum analyzers based on the Discrete Fourier Transform (DFT), as a special case of the time domain approach. This, in our view, may allow to reach a more intuitive and effective understanding of the relevant parameters influencing the estimation process.

Let us start by taking into consideration the sample and hold circuit in Fig. 5. Let us assume that sampling occurs at regular time intervals T_R. We have therefore the samples $v_{sm}(hT_R)$ at the output $v_h(t)$, with $h = 0, 1, \ldots, M - 1$. Instead of using the RHS of Eq. (11) for the estimation of the average power of the process, we can write

$$S_b(f_k)\Delta \mathrm{f} = \frac{1}{M}\sum_{h=0}^{M-1} |v_{sm}(hT_R)|^2 \quad \text{for a sufficiently large } M. \tag{16}$$

Assuming that samples are taken sufficiently apart from each other so that they are uncorrelated, we can estimate the standard deviation in the estimate of $S_{BM}(f_k)$ after M samples using Eq. (14) as follows:

$$\sigma_{SBM} = \frac{S_B(f_k)}{\sqrt{M}} = \frac{S_B(f_k)}{\sqrt{T/T_R}}, \tag{17}$$

where T is, as before, the total measurement time. We obtain that, also with this approach, the standard deviation of the estimate is inversely proportional to the measurement time. We expect, however, that the second approach provides, in general, a larger standard deviation with respect to Eq. (15) because it does not use all the available information. This means that, for obtaining uncorrelated samples, T_R must be, in general, larger than $1/(2\Delta f)$. This is quite reasonable when we think that the PSD of v_{sm} extends from $-\Delta f/2$ to $\Delta f/2$, and hence, the PSD of the squared quantity (we are assuming, for simplicity, a real signal at the output of the low pass filter in Fig. 5) extends from $-\Delta f$ to Δf. Since the PSD of ${v_{sm}}^2$ is the Fourier transform of its autocorrelation function, it assumes, therefore, non-negligible values for times in the range from about $-1/\Delta f$ to $1/\Delta f$. As we shall presently see, it is particularly easy to select $T_R = 1/\Delta f$ in

ublished under an exclusive license by AIP Publishing
MOST WIEDZY Downloaded from mostwiedzy.pl

actual measurements, and this means that a moderate degree of correlation still exists among samples close to one another. Therefore, when we set $T_R = 1/\Delta f$ in Eq. (17), so that we have

$$\sigma_{SBM} = \frac{S_B(f_k)}{\sqrt{\Delta f T}}, \tag{18}$$

we must regard σ_{SBM} as an optimistic estimate, although not too far from the actual experimental results. Moreover, overlapping methods can help in reducing the gap between the standard deviation that can be obtained with continuous integration and the one corresponding to the sampling approach.[101]

Finally, it is worth mentioning that the result in Eq. (15) is only accurate if we employ and ideal low-pass filter and the PSD in the passband is constant. Unfortunately, and ideal low-pass filter such as the one in Fig. 5 cannot be realized, although the overall trend for the standard deviation of the estimate remains the same. When we deal with realistic filter responses, the relationship between the power of the process $v_{sm}(t)$ and the PSD of the process at its input must be written in the form

$$P_{Bm} = \int_{-\infty}^{+\infty} |H(f)|^2 S_{Bk}(f) df. \tag{19}$$

In general, we would like to have $H(f)$ shaped as close as possible to an ideal low-pass filter so that most of the contribution to P_{Bm} comes from a limited frequency interval across DC (across f_k with reference to the PSD before multiplication). What we cannot do, in general, is to obtain a constant value for $H(f)$ in this frequency interval. To recover the simple and intuitive interpretation that is made possible in terms of the ideal low-pass filter, we often resort to the concept of Equivalent Noise Bandwidth (ENB) for a real filter. In particular, assuming as before that most of the contribution to P_{Bm} comes from a frequency interval in which $S_{Bk}(f)$ can be assumed constant, we define the ENB of a filter $H(f)$ as that bandwidth that would allow to obtain the same power P_{Bm} if a an ideal filter with constant amplitude $H(0)$ was used instead of $H(f)$, that is,

$$ENB = \frac{\int_{-\infty}^{+\infty} |H(f)|^2 df}{|H(0)|^2}. \tag{20}$$

With the introduction of *ENB*, and assuming that we ensure $H(0) = 1$, Eq. (11) still holds, provided we replace Δf with the proper value of *ENB*. Note that, for the properties of the Fourier transform, we also have

$$ENB = \frac{\int_{-\infty}^{+\infty} |h(t)|^2 dt}{\left|\int_{-\infty}^{+\infty} h(t) dt\right|^2}. \tag{21}$$

A class of filters that are particularly easy to implement in the numerical domain are Finite Impulse Response (FIR) filters. While these filters are not physically realizable in the continuous time domain, we will, for the time being, neglect this aspect. Let us therefore assume that a continuous time FIR filter is used for the implementation of the low pass filter in Fig. 5 and that, in particular, the duration of the impulse response is equal to the output sampling interval T_R. If this last condition is satisfied, we obtain the very interesting result that the signal $v_{sm}(t)$ at the output of the low pass filter only depends on the value of the input signal in the finite time interval between $t - TR$ and t. Indeed, if $h(t)$ is the impulse response of a hypothetical continuous time FIR filter used in Fig. 5, we have

$$h(t) \neq 0 \text{ only for } 0 \leq t < T_R; \tag{22}$$

therefore,

$$\begin{aligned} v_{sm}(t, f_k) &= \int_{-\infty}^{+\infty} v_s(\tau) e^{-j2\pi f_k \tau} h(t-\tau) d\tau \\ &= \int_{t-T_R}^{t} v_s(\tau) e^{-j2\pi f_k \tau} h(t-\tau) d\tau, \end{aligned} \tag{23}$$

where with the notation $v_{sm}(t,f_k)$ we have explicitly stressed the fact that, for the same $v_s(t)$ at the input of the system, v_{sm} depends on the value of f_k. Let us now assume that we sample the input signal at a frequency much larger than the *ENB* of the FIR filter used in Fig. 5. It means that we sample the impulse response of the filter and the term $\exp(-j2\pi f_k \tau)$ at the same sampling frequency f_S and that we want to employ the sampled values to obtain an estimate of $v_{sm}(t,f_k)$ at regular intervals T_R. To avoid aliasing, the input signal must be low-pass filtered with a bandwidth $B < f_S/2$ and, clearly, it only makes sense to employ values of $|f_k|$ less than $f_S/2$. Calculations become particularly simple if, given the sampling interval $\Delta t_S = 1/f_S$, we have

$$\begin{aligned} &T_R = N\Delta t_S \quad N \text{ natural} > 0, \\ &f_k = \frac{k}{T_R} = \frac{k}{N} f_S \qquad k \text{ integer}; -\frac{N}{2} < k < \frac{N}{2}. \end{aligned} \tag{24}$$

With these assumptions, for the estimation of $v_{sm}(hT_R)$ according to Eq. (23), we have

$$\begin{aligned} v_{sm}(hT_R, f_k) &= \int_{(h-1)T_R}^{hT_R} v_s(\tau) e^{-j2\pi \frac{k}{N} f_S \tau} h(hT_r - \tau) d\tau \\ &\approx \Delta t_S \sum_{i=0}^{i=N-1} v_s[(h-1)T_R + i\Delta t_S] e^{-j2\pi \frac{k}{N} i} w(i\Delta t_S), \end{aligned} \tag{25}$$

where we have made the position

$$w(i\Delta t_S) = h[T_R - i\Delta t_S], \tag{26}$$

and we have used the fact that, because of Eq. (24),

$$e^{-j2\pi \frac{k}{N} f_S [(h-1)T_R + i\Delta t_S]} = e^{-j2\pi \frac{k}{N} i}. \tag{27}$$

This result is extremely important as it shows that $v_{sm}(hT_R, f_k)$ can be estimated, apart from a factor Δt_S, using the very same algorithm that is used for the estimation of the Discrete Fourier Transform (DFT) $Y(k)$ of a N samples sequence y_i,

$$Y(k) = \sum_{i=0}^{N-1} y_i e^{-j2\pi \frac{k}{N} i}; \quad y_i = v_s[(h-1)T_R + i\Delta t_S] w(i\Delta t_S). \tag{28}$$

The sequence $w_i = w(i\Delta t_S)$ is often referred to as window function, and different window functions can be used, although in low-frequency noise measurements the rectangular (or uniform) and the Hanning windows are the most used ones. Note that once the sampling frequency and the number of samples N are chosen, the resolution Δf in the values of f_k that can be chosen is given by

$$\Delta f = \frac{f_S}{N} = \frac{1}{T_R}. \tag{29}$$

ublished under an exclusive license by AIP Publishing
MOST WIEDZY Downloaded from mostwiedzy.pl

Moreover, it turns out that, for the most common window functions, the ENB does not differ much from Δf so that these two parameters (Δf and ENB) can be used, to a certain extent, interchangeably. This means that we can still use Eq. (18) for the estimation of the residual statistic error [in the context in which Eq. (18) was obtained, Δf played the role of the ENB]. The frequency resolution is, of course, also the lowest frequency (other than 0) at which we can obtain an estimate of the noise PSD. This means that if we set a limit to the maximum statistical error that we can accept, we obtain, for the overall measurement time T according to Eq. (18),

$$T > \frac{1}{\Delta f \varepsilon_r^2}; \; \varepsilon_r = \frac{\sigma_{SBM}}{S_B(f_k)}. \tag{30}$$

Suppose we require a residual normalized statistical error of 5% with a minimum frequency of interest of 100 mHz, from Eq. (30), we can calculate that we require an overall measurement time in excess of 1 h (4×10^3 s). This example clearly shows that, when measurement time is limited, a compromise must be found between the minimum frequency of interest and the statistical residual error that can be obtained. If instead of 5% we can accept an error of 10% and we restrict ourselves to frequencies above, say, 200 mHz, the required measurement time reduces to less than 10 min. These estimations only take into account the need for the statistical error to reduce below a certain level, but there is another source of error that must be considered when selecting the frequency resolution Δf. The necessary hypothesis for the estimation for the PSD from the total power collected by a filter divided by the ENB of such filter is that the PSD stays almost constant within the bandwidth of the filter. In the case of LFNM, the typical PSD we are interested in is in the form

$$S_B(f) = \frac{A_B}{|f|^\gamma}; 1 \le \gamma \le 2, \tag{31}$$

where A_B is a proper constant. Incidentally, most often, it is the monolateral PSD $S(f)$ that is used to report experimental results,

$$S(f) = 2S_B(f) = \frac{A}{f^\gamma}; A = 2A_B f > 0. \tag{32}$$

It should therefore be apparent that, with this type of functional dependence on the frequency, it is not really justified to assume $S(f)$ to be constant in a frequency interval Δf. Moreover, since in actual measurements we are dealing with the real filters, their frequency response is not null outside the ENB, and therefore there can be a significant contribution to the power gathered by a filter whose center frequency is low (Δf, $2\Delta f$, etc., corresponding to $k = 1,2$ etc.) from the hugely peaked shape of the spectrum at $f = 0$. Finally, residual DC superimposed to the actual noise signal may still significantly contribute to the power at the output of the filters for low values of k, thus introducing large systematic errors. These sources of errors are analyzed in some detail in Giusi *et al.*[102] As an example, Fig. 6 reports the systematic error that is obtained (in the absence of statistical error) for different values of the exponent γ when the uniform window is used. The error does not depend on the absolute value of the frequencies, but rather on the value of k.[102] This means that if we are interested in a minimum frequency f_{min} = 100 mHz, we can set up the estimation process with $\Delta f = f_{min}$ accepting a systematic error larger than 10% on f_{min} (Fig. 6) or we can set Δf to a smaller

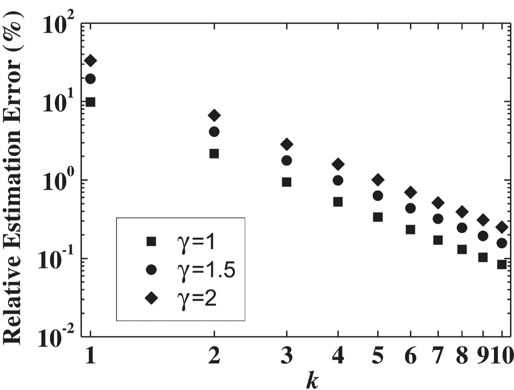

FIG. 6. Relative systematic estimation error (with no statistical error) at frequency points $f_k = k\Delta f$ when the PSD of the noise signal has the form A/f^γ. Reproduced with permission from G. Giusi, G. Scandurra, and C. Ciofi, Fluctuation Noise Lett. **12**, 1350007 (2013). Copyright 2013 World Scientific Publishing.

value, so that f_{min} now corresponds to a larger k. For instance, with $\Delta f = f_{min}/10$, the systematic error at f_{min}, which now corresponds to $k = 10$, becomes a fraction of 1%. Indeed, when all sources of systematic error are taken into consideration, it is generally found that setting $\Delta f = f_{min}/10$ is sufficient to ensure a systematic error that remains well below the residual statistical error in most situations. This choice, however, comes to a high cost in terms of measurement time. If, with the example before (f_{min} = 100 mHz, statistical error less than 5%), we now select $\Delta f = f_{min}/10$, the required measurement time becomes 10 times larger (more than 11 h).

Following the approach discussed in Ref. 102, one could, in principle, estimate beforehand the best measurement parameters for the optimization of the measurement time given certain margins of acceptable errors. The problem is, however, that not all the required parameters for this estimation are known beforehand. The ability to detect systematic errors in LFNM is especially important when the detailed shape of the spectrum is used to verify conduction models or as a footprint for the chemical composition of a gas mixture or a solution in advanced applications, such as Fluctuation Enhanced Sensing (FES).[95]

Since the systematic errors reduce as Δf decreases, there would be a simple approach, at least in principle, to check if such errors are present in an estimated spectrum: if the spectrum was obtained with a given Δf, the measurement can be repeated with a smaller Δf. If the two spectra superimpose at the lowest frequency of interest, we can be reasonably assume that no systematic error is present. If not, we need to repeat the process with lower and lower values for Δf. Clearly, this approach is quite expensive in terms of measurement time and effort. An equivalent approach would be to employ several spectrum analyzers in parallel, each set with a different Δf. In this case, the spectrum analyzer with the largest Δf would be the one providing the spectrum with a very low statistical error in the shortest time; the spectrum analyzer with the next smaller Δf would be affected by smaller systematic errors, but, at the same time, the statistical error would be larger for the same measurement time with respect to the first one. If we notice difference

MOST WIEDZY Downloaded from mostwiedzy.pl

ublished under an exclusive license by AIP Publishing

in the spectra estimated at the lowest frequency of interest, we conclude that systematic error is present, and we will have to check for the spectra with the next smaller Δf to see if the second (smaller) value of Δf is sufficient for the required accuracy. This process can continue and, clearly, any time we move to the spectrum analyzer with the next smaller Δf, we need to accept the fact that a longer measurement time will be required to reach the desired level of statistical accuracy. With respect to the previous approach, however, no time is wasted (measurements are carried out in parallel). However, employing several benchtop spectrum analyzers in parallel would be quite expensive and it is for this reason that in the past few years a software library that behaves equivalently to a number of spectrum analyzers in parallel with decreasing Δf has been developed.[103] It was designed with the goal, among others, of addressing the very issues that we have just described. Although not anyone might be willing to employ software libraries developed by others for the development of dedicated spectrum analyzers, we hope that in this section we have helped in demystifying the process employed for the estimation of PSD from the sampled version of the signal to be analyzed. While a conventional spectrum analyzer is a quite convenient piece of instrumentation to have available in any laboratory, we strongly feel that devoting some effort in the development of customizable spectrum analyzers as can be obtained by employing proper acquisition boards and by developing proper software can result in an important tool in the development of measurement systems for advanced LFNM.

III. LOW IMPEDANCE DEVICE UNDER TEST

As we have discussed in Sec. II A, when we have to deal with low impedance devices, we preferably employ the measurement configuration in Fig. 3(a), with a bias resistance R_B much larger than the DUT impedance and a proper value for V_B, so that the bias circuit essentially behaves as an ideal current source and the noise voltage across the DUT coincides with its internal equivalent voltage noise source. If no bias is applied to the DUT, only thermal noise is present at its ends, which carries no information about the internal conduction mechanisms. In order to excite excess noise, the DUT needs to be biased with a sufficiently large current so that the flicker noise overcomes the thermal noise component. Since the PSD of flicker noise is inversely proportional to the frequency as in Eq. (32) (with exponent coefficient γ typically ranging between 1 and 2), in principle, it could be detected at very low frequencies with a vanishingly small bias. In practice, since there is a limit to the minimum frequency that can be explored in a reasonable time, the bias needs to be increased until the flicker noise is sufficiently large to overcome the thermal noise in the lowest frequency range that can be observed. Actually, since also the amplifier connected to the DUT introduces flicker noise, the DUT bias must be increased so that the noise produced by the DUT overcomes the overall background noise of the system. Based on these observations, it should be clear that in order to maximize sensitivity, we should be able to operate down to the lowest possible frequencies with the lowest possible background noise. It is generally the case that a sufficiently large bias can lead to a detectable flicker noise level even in the case of relatively large background noise, but this comes at a cost. Consider, for instance, the case of LFNM applied to the investigation of electromigration in IC metallic lines.[104] Exciting electromigration noise requires that the lines be stressed with high temperature and high current densities that generally result in accelerated stress with respect to actual operating conditions. From the point of view of the investigation of the degradation mechanisms, the degree of over-stress should be as moderate as possible, in order to avoid that the tests are performed in a completely different degradation regime with respect to the one occurring at normal operating conditions. Clearly, the amount of over stress required to make electromigration noise detectable depends both on the lowest frequency range that can be investigated and on the level of background noise. It was indeed argued that the large spread in electromigration noise behaviors reported by different research groups can be correlated with the different sensitivity in the available instrumentation for performing LFNMs.[33] It is therefore obvious that when the stress on the DUT needs to be minimized, it is mandatory to reduce the BN of the system as much as possible and to extend measurements down to lowest possible frequency range. We have already observed, in the previous paragraph, how 100 mHz has to be regarded as a practical lower limit in most cases (for measurements that need to be completed within a couple of hours at most), and therefore we will assume this as the lowest limit in the discussion that follows. Extending LFNM down to even lower frequencies is not impossible, but it is quite rare due to the extremely long measurement times that would be required.

Low noise voltage amplifiers for performing LFNM are commercially available, but the lowest levels of background noise reported in the literature are obtained by resorting to custom designs.[105] Besides a very low noise, what we require, from a low noise voltage amplifier to be used for LFNM in a research laboratory, is a stable and known gain, and for this reason, many designs resort to an operational amplifier (OA) in a shunt-series feedback configuration. To obtain the lowest possible levels of background noise, the operational amplifier is not a standard monolithic device, but it is obtained by resorting to a discrete component differential input stage followed by a gain stage based on monolithic components. Generally, a single stage is not sufficient to provide the required voltage gain (that is typically in excess of 60 dB) so that a two stages configuration (Fig. 7) is used. In Fig. 7, *SOA* is the *Super* Operational Amplifier (SOA) based on a discrete component input stage and the gain A_{V1} is set to $(1 + R_2/R_1)$ because of the shunt-series feedback configuration. Even in the case of a negligible DC at the input v_{in}, because of the presence of the discrete components in the input stage, the DC voltage at the output of the first stage can be quite large and a DC coupling to the II stage would almost certainly results

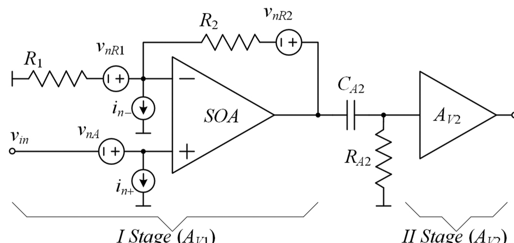

FIG. 7. Basic structure of a low noise voltage amplifier for low frequency noise measurements. *SOA* is typically a "Super" Operational Amplifier obtained with a discrete-devices based input stage.

ublished under an exclusive license by AIP Publishing
MOST WIEDZY Downloaded from mostwiedzy.pl

in saturation. For this reason, the second stage is generally AC coupled to the first stage with a cut in frequency $f_A = 1/(2\pi R_A C_A)$ well below the minimum frequency of interest for LFNM. With a proper design, because of the gain of the first stage (typically in the order of 40 dB), the relevant noise sources setting the background noise of the system reduce to those shown in Fig. 7 that it the thermal noise introduced by the resistances of the feedback network, the Equivalent Input Voltage Noise (EIVN) v_{nA} at the input of the SOA, and the Equivalent Input Current Noise (EICN) sources i_{n+} and i_{n-} at the non-inverting and inverting inputs of the SOA, respectively.[106]

Since we are interested in low frequencies, we can work in the assumption of virtual short circuit between the inputs of the operational amplifier. In order to simplify the discussion, we will also assume all noise sources indicated in Fig. 7 to be uncorrelated. If a DUT with impedance Z_D in series with a voltage noise source v_{Dn} is connected between the input v_{in} of the low-noise amplifier and ground, in the passband of the system ($f \gg f_A$) we have, for the PSD S_{Vo} of the voltage noise at the output,

$$S_{Vo} = \left[\left(S_{vD} + S_{vnA} + S_{in+}|Z_D|^2\right)|A_{V1}|^2 + \left(S_{in-}R_2^2 + 4kTR_2 + 4kTR_1\frac{R_2^2}{R_1^2}\right)\right]|A_{V2}|^2, \quad (33)$$

where S_{vD}, S_{vna}, S_{in+}, and S_{in-} are the PSDs of the noise sources v_{Dn}, v_{nA}, i_{n+}, and i_{n-}, respectively; $4kTR_1$ and $4kTR_2$ are the PSD of the thermal noise introduced by R_1 (v_{nR1}) and R_2 (v_{nR2}), respectively, where k is the Boltzmann constant and T is the absolute temperature.

A useful way to deal with the noise introduced by an amplifier (actually by any two port circuit) is to resort to the representation in Fig. 8, where the amplifier in Fig. 7 is represented as a noiseless two port device with two equivalent noise sources v_n and i_n, both independent of the source impedance.[107] If we can assume v_n and i_n to be uncorrelated and $Z_{in} \to \infty$ (as it is reasonable for a voltage amplifier at low frequencies), the PSD S_{Vo} of the output noise can be calculated as

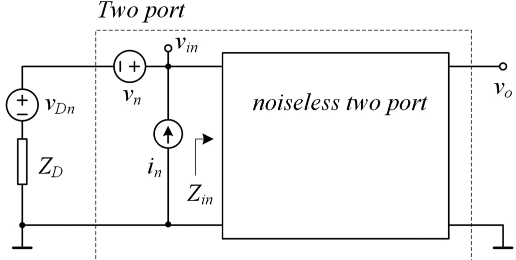

FIG. 8. Representation of a noisy two-port by means of a noiseless two-port with equivalent input current and voltage noise sources at its input. The equivalent noise sources at the input are independent of the source impedance Z_D.

$$S_{Vo} = (S_{vid} + S_{iBN})|A_V|^2; S_{iBN} = S_{vn} + S_{in}|Z_D|^2, \quad (34)$$

where we have indicated with S_{iBN} the equivalent input background noise. For Eq. (34) to be equivalent to Eq. (33), it is sufficient to make the following positions:

$$S_{in} = S_{in+}; \quad S_{vn} = S_{vnA} + \frac{1}{|A_{V1}|^2}\left(S_{in-}R_2^2 + 4kTR_2 + 4kTR_1\frac{R_2^2}{R_1^2}\right); \quad A_V = A_{V1}A_{V2}. \quad (35)$$

Since A_{V1} is typically much larger than one, a quite insightful expression for S_{vn} can be obtained if we make the approximation $A_{V1} \approx R_2/R_1$,

$$S_{vn} = S_{vnA} + S_{in-}R_1^2 + 4kTR_1. \quad (36)$$

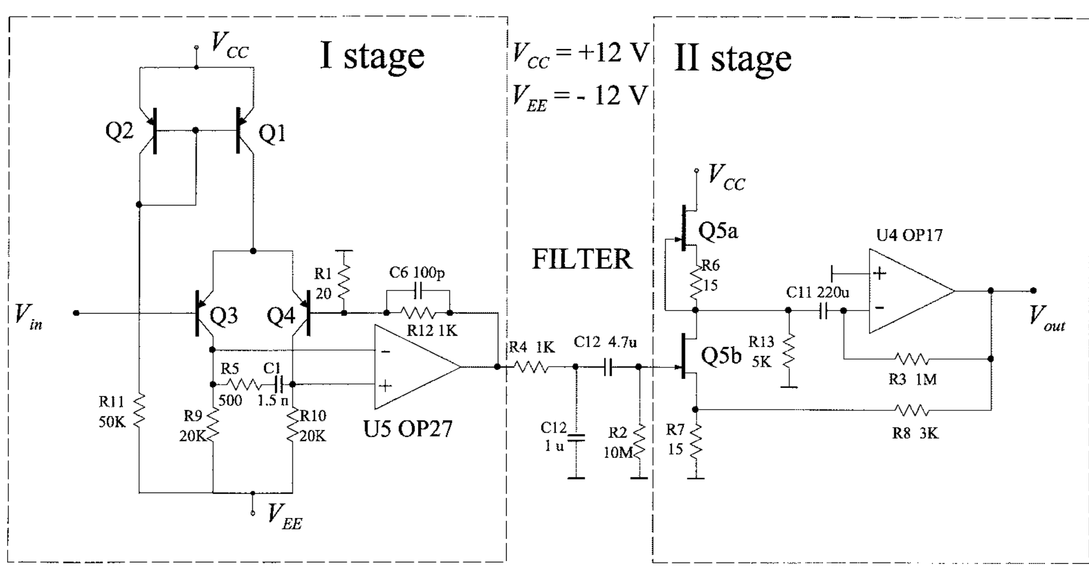

FIG. 9. Schematic of an ultralow-noise preamplifier using a differential input stage based on discrete low noise SSM2220 BJTs. Reprinted with permission from C. Ciofi, M. de Marinis, and B. Neri, IEEE Trans. Instrum. Meas. **46**, 789–793 (1997). Copyright 1997 IEEE.

MOST WIEDZY Downloaded from mostwiedzy.pl

As far as the value of R_1 is concerned, what matters is that the ratio R_2/R_1 provides the desired value for the gain. This means that, in principle, R_1 can be made as small as required in order to reduce S_{vn} down to the contribution S_{vnA} only. In actual implementations, however, R_1 cannot be smaller than a few ohms. Otherwise, the parasitic resistances along the printed circuit board traces may result in a deviation of the actual gain from the design value. At room temperature, the thermal noise of 10 Ω resistance is about 168×10^{-21} V^2/Hz or 0.4 nV/$\sqrt{}$Hz. This noise level can be relevant in setting the BN level at frequencies higher than a few Hz, where the flicker noise component of S_{vnA} becomes negligible. Notwithstanding, at lower frequencies ($f < 1$ Hz), the thermal noise from the resistance R_1 is typically negligible.[108] As far as the contribution from the current noise sources at the inputs of the SOA is concerned, one of them (i_{n+}) sets the equivalent current noise in the two-port representation in Fig. 8, while the other contributes to the equivalent voltage noise. In many designs, the current noise sources in Fig. 8 coincide with the equivalent input current noise sources at the control terminals of the active devices used in the discrete component front end stage, which is the gate in case of JFET devices, or the base in the case of BJT devices. It turns out that there is a huge difference in the level of current noise observed in the case of BJTs and JFETs, as there is a huge difference in the value of the bias current at the base and at the gate for the two devices. In a nutshell, the effect of the current noise at the gate of a JFET, with a proper design, can be almost always neglected with respect to other sources of noise, while in the case of BJTs the contribution from S_{in} to the S_{iBN} in Eq. (34) can be relevant for impedances larger than a few tens of ohms. As far as the equivalent input voltage noise v_{nA} is concerned, with a proper design, it can be reduced to the contribution of the active devices in the input stage and, for a differential configuration, its PSD is twice that corresponding to the equivalent input voltage noise of a common emitter (for BJTs) or a common source (for JFETs) configuration. For the same bias (collector current or drain current for BJT and JFETs, respectively), BJTs have lower equivalent voltage noise and larger transconductance gain with respect to JFETs. For instance, each of the two low noise BJTs in the SSM2220 integrated circuit, when biased with 1 mA of collector current, are characterized by a transconductance gain of 30 mA/V and an equivalent input voltage noise level of about 1.5 nV/$\sqrt{}$Hz at 100 mHz,[109] whereas for a low noise JFET 2SK170, at the same drain current, we have a transconductance of 14 mA/V and an equivalent (extrapolated) input voltage noise about 30 nV/$\sqrt{}$Hz.[110] An example of a BJT input ultra-low noise amplifier is shown in Fig. 9, with the corresponding PSD for the equivalent input voltage and current noise sources reported in Fig. 10.[111]

The bias network (R_{11}, Q_2, and Q_1) sets the bias current for the input differential stage (Q_3 and Q_4 SSM220 transistors) to about 2.5 mA per transistor; the gain of the first stage is set to $1 + R_{12}/R_1$, which is about 50 (or 34 dB). The network R_5C_1 introduces a zero-pole compensation to ensure stability. The second stage is obtained as a cascade of a transconductance stage based on discrete JFETs followed by a transimpedance stage in a shunt-series configuration with a gain set to $1 + R_8/R_7$, which is about 200 for an overall gain of 10^4 (or 80 dB). The interstage AC filter ($C_{12}R_2$) has a lower corner frequency of 3.4 mHz. The performances in terms of EIVN and EICN are shown in Fig. 10 (curve 1 and 2, respectively). It can be noticed that at 100 mHz we obtain an equivalent input noise voltage level of about 10^{-17} V^2/Hz (or 3.2 nV/$\sqrt{}$Hz) that is among the lowest ever reported for this type of instrumentation. As observed before, the equivalent input noise voltage sets the background noise as long the effect of the EICN is negligible. As it can be seen in Fig. 10 (curve 2), at 100 mHz, the EICN is about 2×10^{-21} A^2/Hz (or 45 pA/$\sqrt{}$Hz), and this means that the EICN produces a noise larger than the EIVN for source impedances above about 70 Ω (45 pA/$\sqrt{}$Hz × 70 Ω = 3.15 nV/$\sqrt{}$Hz). The relatively large value of EICN is also the reason why this amplifier needs to be DC coupled to the DUT, which, in turns, sets a limit to the DC voltage that can be present across the DUT during measurements. With a gain of 50 for the first stage, the limit to the input DC voltage range is about ±100 mV, which can be insufficient in some applications. One may argue that since the amplifier is AC-coupled in any case (there is an AC filter between the first and the second stage), perhaps it may be possible to introduce an AC coupling network, similar to the one used between the first and the second stage, to reject the DC component across the DUT. This approach, however, is not feasible, at least in the case of BJT input amplifiers because of the large EICN. In order to better understand this issue, we can refer to the equivalent circuit in Fig. 11. The interposition of the AC coupling filter (ACC) between the DUT and the input of the amplifier has two main consequences, as far as the background noise is concerned: (a) the resistance in the filter introduces noise and (b) the presence of the filter changes the source impedance seen by the input of the amplifier.

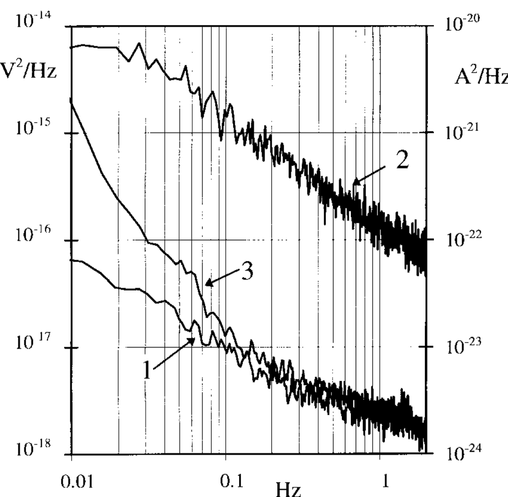

FIG. 10. PSD of the equivalent input voltage noise (curve 1) and equivalent current noise (curve 2) of the amplifier in Fig. 9. Curve 3 shows the apparent increase in the PSD of the equivalent input voltage noise when electromagnetic interferences leak in the measurement chamber because of incomplete shielding. Reprinted with permission from C. Ciofi, M. de Marinis, and B. Neri, IEEE Trans. Instrum. Meas. **46**, 789–793 (1997). Copyright 1997 IEEE.

The noise contribution from R_A depends on the DUT impedance and on the frequency. It must be noted, however, that in order not to attenuate the noise signal coming from the DUT, R_A must be much larger than all possible $|Z_D|$ to be investigated at all frequencies of interest. This means that, for the noise signal v_{nRAin} at the input of the amplifier due to the noise source v_{nRA}, we have

MOST WIEDZY Downloaded from mostwiedzy.pl

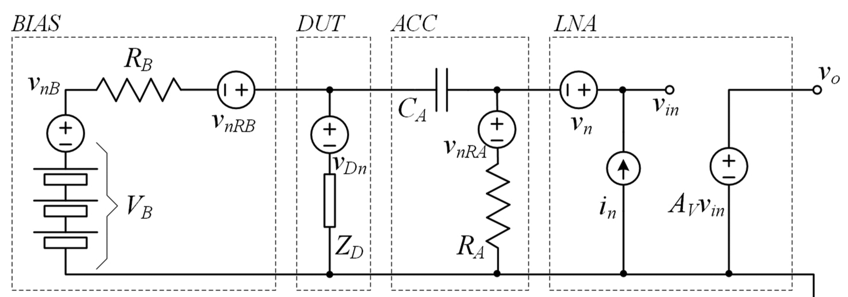

FIG. 11. Equivalent circuit for the calculation of the effects of the input AC coupling filter (ACC) on the background noise of the system.

$$v_{nRAin} \approx \frac{Z_D + \frac{1}{j2\pi f C_A}}{Z_D + \frac{1}{j2\pi f C_A} + R_A} v_{nRA} \approx \frac{1}{1 + j2\pi f C_A R_A} v_{nRA}$$
$$= \frac{1}{1 + \frac{jf}{f_A}} v_{nRA}; \quad f_A = \frac{1}{2\pi C_A R_A}, \tag{37}$$

where f_A is the cut in the frequency of the filter that must be obviously much smaller than the minimum frequency of interest. Therefore, we have, in terms of the PSD S_{nRAin} of v_{nRAin},

$$S_{nRAin} \approx S_{nRA}\left(\frac{f_A}{f}\right)^2 = 4kTR_A\left(\frac{f_A}{f}\right)^2 = \frac{1}{f^2} \times \frac{kT}{\pi^2 C_A^2 R_A}. \tag{38}$$

From Eq. (38), we notice that the larger contribution to the noise is obtained at the lowest frequency of interest and that, for the same capacitance C_A, the larger the resistance, the better. Typically, in order to avoid micro-discharge phenomena that would result in artifacts in the measured spectra, the capacitances to be used in the *AC* filter must be high rated voltage polyester or polypropylene capacitors that can be obtained, in reasonable sizes, up to a few tens of microfarads. Let us assume that we have $C_A = 10\ \mu$F. In order to satisfy the condition $f_a < f_{min}$ ($f_{min} = 100$ mHz), a resistance R_A in excess of 150 kΩ would be sufficient, but in order to obtain a noise contribution from R_A smaller that the EIVN of the amplifier in Fig. 9 at 100 mHz (10^{-17} V^2/Hz), the resistance R_A must be in excess of 40 MΩ. This would result in a cut in frequency well below 1 mHz, with the adverse effect of very long transients any time the bias across the DUT is changed. The real problem, however, comes when we now take into consideration the consequences of the introduction of such an AC filter as far as the effect of the EICN of the amplifier in Fig. 9 is concerned. With the same approximations used to obtain Eq. (38) (that is very small DUT impedance and minimum frequency of interest well above the cut in frequency of the AC filter), the impedance seen by the input of the amplifier would essentially reduce to the impedance of the capacitance C_A that is maximum at the minimum frequency of interest. Assuming 100 mHz as the minimum frequency of interest and $C_A = 10\ \mu$F, we have that its impedance at f_{min} is in excess of 150 kΩ, which, with an EICN of 45 pA, would be equivalent to the presence of a voltage noise source at the input in the order of 7 μV/$\sqrt{\text{Hz}}$: this noise, in terms of PSD, would be more than 6 orders of magnitude larger than the intrinsic EIVN of the amplifier. In the case of BJT input ultralow-noise amplifiers, therefore, other methods need to be used to deal with the DC component at the input. A possible solution is to resort to a bridge configuration as in Fig. 12. By taking advantage of the fact that independent batteries can be used to bias the bridge and to supply the amplifier, the ground connection of the amplifier can be connected to the node (a) of the bridge as in Fig. 12, and by a proper adjustment of the variable resistance R_V, the DC voltage at the input of the amplifier can be essentially nulled. Note that a clear disadvantage of this configuration is the fact that the resistance R_V becomes part of the DUT and the noise introduced by R_V adds to the background noise of the system. If excess noise free resistances are used for R_V when dealing with the flicker noise components from the DUT this might not be a problem. In some cases, however, it is possible to connect a second DUT (nominally identical to the other) so that we essentially double the useful noise signal by measuring two samples at the same time.

As it is apparent, dealing with BJT input low-noise amplifiers, because of the need for DC coupling to the DUT, can be quite complicated. From this point of view, dealing with JFET input low-noise amplifiers could be much easier, since in this case, because of the very small level of EICN for these devices, AC coupling to the DUT is seldom a problem. Note that the second stage of the amplifier in Fig. 9 can be regarded as a low-noise, JFET input amplifier that is AC coupled to the noise source by means of the AC filter $C_{12}R_2$. The topology of the second stage of the amplifier in Fig. 9 is indeed the basis for a number of ultralow-noise JFET input amplifiers reported in the literature.[105,112,113]

From Fig. 9, it could be argued that designing a custom ultra now noise amplifier is not a straightforward process, since a large number of components are required and obtaining stable operation can be a quite difficult task. However, obtaining excellent noise performances is not necessarily a synonymous of large circuit complexity. For instance, the ultralow-noise amplifier developed in

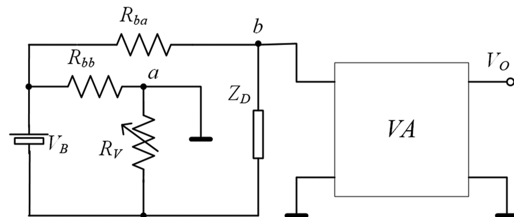

FIG. 12. Bridge bias configuration for DC coupling to a low noise amplifier. R_V must be adjusted to minimize the DC voltage between nodes *a* and *b* in order to avoid saturation of the voltage amplifier *VA*.

ublished under an exclusive license by AIP Publishing
MOST WIEDZY Downloaded from mostwiedzy.pl

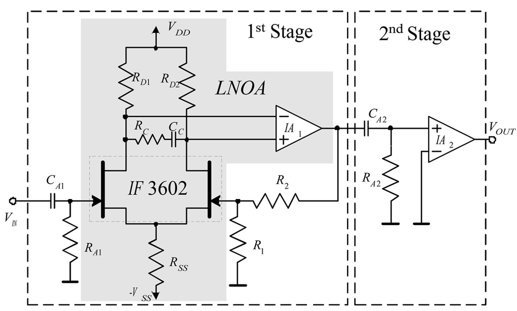

FIG. 13. An ultralow-noise voltage amplifier with an input stage based on low noise discrete JFETs. Notwithstanding the simple topology and the low component count, the amplifier is characterized by excellent noise performances. Reproduced with permission from G. Cannatà, G. Scandurra, and C. Ciofi, Rev. Sci. Instrum. **80**, 114702 (2009). Copyright 2009 AIP Publishing LLC.

Cannatà *et al.*[108] whose schematic is reproduced in Fig. 13, was prepared with ease of reproduction in mind. As it can be noticed, the component count is very low while the performances in terms of EIVN, as reported in Fig. 14, are excellent, for a JFET input amplifier. As an example of the gain that can be obtained in terms of reduced background noise, the EIVN of the commercial SR560 low-noise amplifier at 1 Hz (that is at the lowest frequency specified by the manufacturer) is about 30 nV/$\sqrt{}$Hz (0.9×10^{-15} V^2/Hz), while in the case of the amplifier in Fig. 13, at the same frequency, the noise level is 1.4 nV/$\sqrt{}$Hz (20×10^{-18} V^2/Hz), with a gain in sensitivity of more than 26 dB. A fully differential input version of the circuit in Fig. 13 can be also built to allow noise measurements in a four wires configuration.[114]

A circuit technique that is often employed to further reduce the EIVN with respect to the one resulting from the characteristics of the input active devices is that of connecting several of such devices in parallel when designing the front end of a low-noise voltage amplifier. This approach can be effective both in the case of BJT input stages[109] and in the case of JFET input stages.[112,113] Assuming, as it

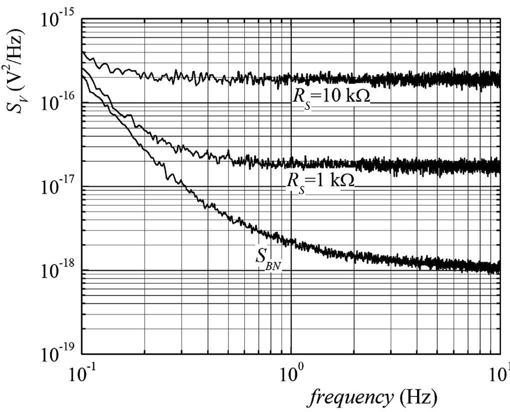

FIG. 14. Equivalent input noise measured with the amplifier in Fig. 13 with the input shorted (curve S_{BN}) and when a 1 kΩ and 10 kΩ resistors are connected to the input. Reproduced with permission from G. Cannatà, G. Scandurra, and C. Ciofi, Rev. Sci. Instrum. **80**, 114702 (2009). Copyright 2009 AIP Publishing LLC.

is reasonable, that the noise sources associated with each device are uncorrelated, with reference to Fig. 15, we have that the parallel connection of number M JFETs is equivalent to a *Super* JFET with PSDs S_{eneq} and S_{ineq}, for the equivalent noise sources v_{neq} and i_{neq}, given by

$$S_{eneq} = \frac{S_{en}}{M}; \quad S_{ineq} = MS_{in}, \tag{39}$$

where S_{en} and S_{in} are the PSDs of each of the equivalent voltage sources v_{ni} and equivalent current source i_{ni} at the input of each single device. This approach is effective as long as the EIVN remains the most relevant contribution to the BN notwithstanding the increased level of EICN. It must also be noted that paralleling M devices means employing an overall bias current that is M times larger. This might be a problem not only because, with battery-operated system, the autonomy is reduced but also because of the increased power dissipation that can create air convection in close proximity with the input devices and increase the background noise because of additional fluctuations due to thermal effects. Finally, paralleling M devices also results in an increase, by the same factor, of the input capacitance, and this can lead to an unacceptable reduction of the bandwidth.

Paralleling devices in order to reduce the EIVN, at the cost of an increase in the EICN, can be also obtained by directly paralleling the inputs of amplifier and combining the output with a proper network. This approach is effective when the amplifiers are very simple and have small dimensions. Indeed, a modular approach that allows us to combine voltage amplifiers based on operational amplifiers (without discrete components) in order to reach EIVN levels compatible with high sensitivity LFNM has been demonstrated.[115] The modularity, in this case, helps in balancing the desired level of BN with the magnitude of the input capacitance, depending on the nature and characteristics of the DUT.

Another possible approach for reducing the EIVN of a given amplifier is that of employing a signal transformer interposed between the DUT and the actual input of the amplifier, as shown in Fig. 16.[73] Within the pass-band of the transformer, the EIVN and the EICN seen at the input of the transformer (v_{AB} in Fig. 16) are modified as in Eq. (39) with M equals to the turn ratio n squared ($M = n^2$). Note, however, that the transformer also introduces noise (e_{nT1} in Fig. 16) due to the parasitic resistance of the primary winding that, for transformers to be employed at very low frequencies (below a few Hz), may be in the order of a few ohms. The bridge configuration is necessary to compensate for the DC drop across the DUT (R_{DUT} in Fig. 16) since no DC voltage can be present at the input of the transformer. The presence of the bridge, besides complicating the set-up procedure (any time the bias is changed, for non-linear DUTs, R_v needs to be adjusted to null the DC component of V_{AB}), causes the increase of the background noise because of the thermal noise introduced by R_V, as we have discussed before. It has however been shown that the bridge connection can be avoided by employing a supercapacitor as a DC blocking device.[116] It must be noted that noise in supercapacitors depends on the phenomena occurring in the electrode–electrolyte interface. A thorough model of noise phenomena within this interface was proposed by Hassibi *et al.*[117] Flicker noise in healthy and charged supercapacitors is generally not observed due to its low intensity as in other electrochemical devices (e.g., healthy and charged batteries). While effective in specific cases,

ublished under an exclusive license by AIP Publishing
MOST WIEDZY Downloaded from mostwiedzy.pl

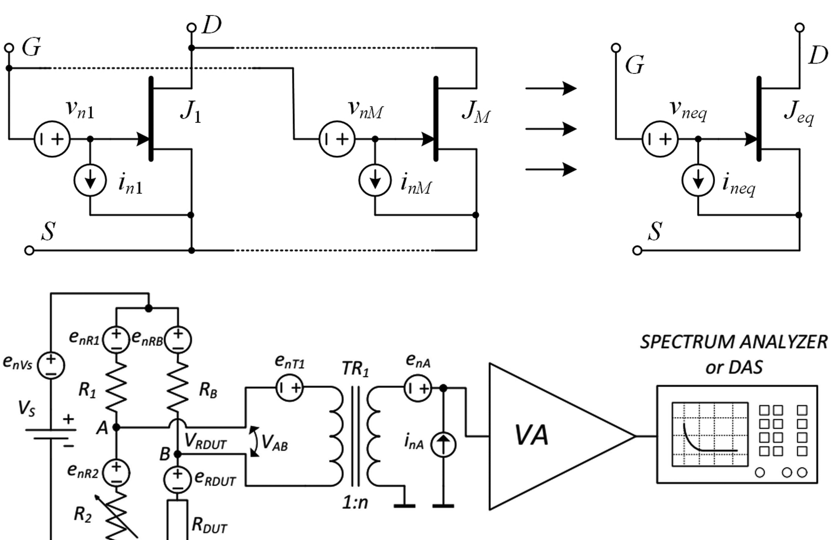

FIG. 15. Parallel connection of several JFETs devices for obtaining an equivalent JFET (J_{eq}) with lower equivalent input voltage noise.

FIG. 16. A low noise voltage amplifier with transformer coupling at the input. Reprinted with permission from Achtenberg *et al.*, Measurement **190**, 110657 (2022). Copyright 2022 Elsevier.

transformers to be employed in LFNM are bulky pieces of equipment and, besides, commercial availability for such devices appears to be quite limited.

Reduction of the EIVN can also be obtained without modifying the available hardware, provided that at least two distinct and nominally identical voltage amplifiers can be connected to the DUT as in the simplified diagram in Fig. 17, by resorting to the properties of cross-correlation.[118–120] At the outputs v_{o1} and v_{o2} we have

$$\begin{aligned} v_{O1} &= v_c + v_{i1} \\ v_{O2} &= v_c + v_{i2}, \end{aligned} \tag{40}$$

where

$$v_c = A_V[v_{iD} + (i_{n1} + i_{n2})Z_D]; \quad v_{i1} = A_V v_{n1}; \quad v_{i2} = A_V v_{n2}. \tag{41}$$

This means that the outputs v_{o1} and v_{o2} are the sum of a common component (v_c) a different uncorrelated component v_{i1} and v_{i2} is added to each of them. In this situation, the mathematical cross spectrum S_{O12} between the noise signals at the outputs of the amplifiers would be

$$S_{O12} = |A_V|^2\left[S_{iD} + (S_{in1} + S_{in2})|Z_D|^2\right]. \tag{42}$$

This mean that, if the contribution from the current noise sources at the input of the amplifiers can be neglected with respect to S_{iD}, by taking the cross spectrum between the two outputs, we can estimate the noise generated by the DUT while completely rejecting the contribution of the noise sources at the inputs of the amplifiers, no matter how large their PSD. This is a quite interesting approach, and in favorable conditions, the noise generated by the DUT can be correctly estimates even if its PSD happens to be orders of magnitude below that of the equivalent input voltage noise of the amplifiers.

The way in which the cross spectrum can be estimated in actual experiment is quite similar to the way in which the power spectrum is estimated. In power spectrum estimation, as discussed before, after calculating the DFT $Y(k)$ of the sequence y obtained applying a proper window to an input sequence of length N, the squared modulus $|Y(k)|^2 = Y(k)\,Y^*(k)$, apart from a proper scale factor, represents an estimate of the PSD of the noise signal at the frequency f_k. In the case of cross spectrum estimation, we start from the sequences y_1 and y_2 obtained applying the same window to the simultaneously sampled signals at input 1 and input 2. After calculating the DFTs $Y_1(k)$ and $Y_2(k)$, the quantity $Y_{12}(k) = Y_1(k)\,Y_2{}^*(k)$, apart for a proper scale factor, represents an estimate of the cross spectrum S_{O12} at the frequency f_k. As in the case of the PSD estimation, averaging

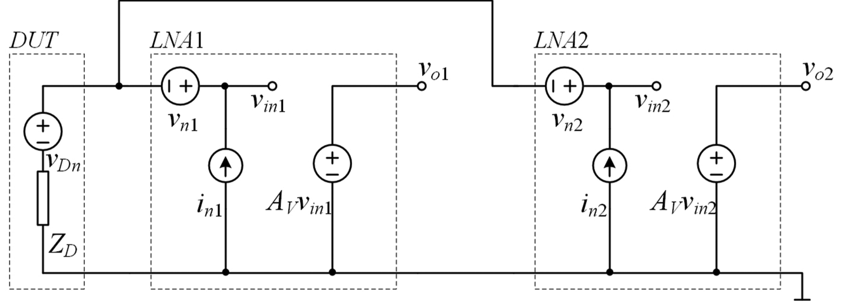

FIG. 17. Measurement configuration for exploiting the properties of cross correlation. The DUT is connected at both the inputs of two nominally identical voltage amplifiers.

MOST WIEDZY Downloaded from mostwiedzy.pl

$Y_{12}(k)$ over a number of sequences is necessary in order to reduce the error in the estimate. The fact is that, in the case in which the uncorrelated noise component is dominant with respect to the correlated one, that is, with reference to the example before (and assuming $S_{in1} = S_{in2} = 0$ for the sake of simplicity), in the case in which we have

$$S_{en1} \approx S_{en1} = S_{en}; S_{en} \gg S_{iD}, \tag{43}$$

the error S_{err} in the estimate of S_{iD} decreases with the number M of records according to[118]

$$S_{err} = \frac{S_{en}}{\sqrt{M}}. \tag{44}$$

As we have discussed before, the time required to perform M records depends on the resolution bandwidth Δf chosen for the estimate of the PSD or of the cross spectrum. Let us assume that we start with S_{en} ten times larger than S_{iD} and that, as in the example at the end of Sec. II, we select f_{min} = 100 mHz and $\Delta f = f_{min}/10$ = 10 mHz (record length = 100 s); if we require S_{err} to reduce to 5% of S_{iD}, we need a reduction factor of 200 that can be obtained with $M = 4 \times 10^4$, with a required measurement time in excess of 46 days! This example serves as a warning about the fact that cross correlation, because of the very long measurement times that are involved, can only be moderately useful in noise measurements at very low frequencies and that even when applying cross correlation, is it extremely important to start with amplifiers characterized by the lowest possible level of background noise. Note that the cross-correlation approach can be extended to the case of $H > 2$ amplifiers connected to the DUT,[121] obtaining a reduction in the residual error, with respect to the case of $H = 2$ and for the same measurement time, by a factor r_H,

$$r_H = \sqrt{\frac{H(H-1)}{2}}. \tag{45}$$

The techniques briefly discussed earlier can be combined together to minimize the background noise in specific situations. For instance, cross correlation applied to a pair of transformers coupled low-noise amplifier has been proven to be effective for the characterization of the low-frequency noise in very low equivalent resistance infrared detectors.[73] The possibility of combining amplifier paralleling and cross correlation to more than two amplifiers connected to the DUT has also been investigated.[122]

IV. HIGH IMPEDANCE DEVICE UNDER TEST

When dealing with the DUT of high impedances, the DUT is biased at a constant voltage and the current fluctuations are typically amplified by means of an operational amplifier (OA) based transimpedance stage as in Fig. 18(a). Save that for special cases, that will be discussed later on, there is usually no need for discrete-device based input stages and a number of easily available off-the-shelf operational amplifiers can be used in the circuit in Fig. 18(a). For biasing the DUT at the desired DC voltage $V_D = V_B$, we take advantage of the virtual short between the inputs of the OA. The alternative configuration in Fig. 18(b) can be used, in which case we have $V_D = -V_B$. Both configurations are used in actual measurements. The main difference between the two is that in the case of Fig. 18(a) the bias current is supplied by the bias source V_B, while in the second case V_B supplies only the bias current to the non-inverting input of the OA. Because of this, it is easier to filter the noise at the output of V_B by interposing a simple passive filter between V_B and the non-inverting input. On the other hand, we have, for the DC voltages V_{TOA} and V_{TOB} at the output of transimpedance stage with the input configuration in Figs. 18(a) and 18(b), respectively,

$$V_{TOA} = -\frac{R_R}{R_D}V_B; \quad V_{TOB} = \left(1 + \frac{R_R}{R_D}\right)V_B; \quad R_D = Z_D(f \to 0). \tag{46}$$

From Eq. (46), it is apparent that $|V_{TOA}|$ is always smaller that $|V_{TOB}|$, and this means that, for the same dynamic range of the OA, the interval of possible values for V_B in the configuration in Fig. 18(a) is larger than that for the configuration in Fig. 18(b). As we have done in the case of the voltage amplifier, we can obtain, from Fig. 18(a), an estimate of the PSD of the equivalent input voltage and current noise sources in the representation in Fig. 18(c) in terms of the noise sources associated with the operational amplifier, to the feedback resistance R_R and to the bias sources. As before, we will assume that all noise sources are uncorrelated, which we are operating at frequencies above the cut-in frequency $f_{cin} = 1/(2\pi C_{A2}R_{A2})$ of the AC coupling filter $C_{A2}R_{A2}$ and that the gain $A_{R1} = -R_R$ (calculated with respect to the noise signal i_{Dn}) of the transimpedance stage is sufficiently large to make the noise contribution of the AC filter and of the second stage negligible. With respect to the case of the voltage amplifier discussed before, we have the complication that even with all noise sources uncorrelated in Fig. 18(a), the equivalent sources v_n and i_n in Fig. 18(c) are not uncorrelated. In order to obtain the correct expression for the background noise we will proceed by ideally replacing the noise sources with deterministic sources so that we can obtain the transfer function from each noise source toward the output of the amplifier. Exploiting the equivalent representation in Fig. 18(c), we have

$$v_o = (i_{Dn} + i_n + v_n Y_D)A_R; \quad Y_D = \frac{1}{Z_D}; \quad A_R = -R_R A_{V2}. \tag{47}$$

For the input configuration in Fig. 18(a), we have

$$i_{n\alpha} = -i_{n-} - \frac{v_{nOA}}{R_R} - \frac{v_{nRR}}{R_R}; \quad v_{n\alpha} = v_{nB} - v_{nOA}, \tag{48}$$

where $i_{n\alpha}$ and $v_{n\alpha}$ are the expressions to be used in Eq. (47) for i_n and v_n, respectively.

In the case of the alternative bias circuit in Fig. 18(b), we have

$$i_{n\beta} = -i_{n-} - \frac{v_{nOA}}{R_R} - \frac{v_{nRR}}{R_R} - \frac{v_{nB}}{R_R}; \quad v_{n\beta} = -v_{nB} - v_{nOA}, \tag{49}$$

where $i_{n\beta}$ and $v_{n\beta}$ are the expressions to be used in Eq. (47) for i_n and v_n, respectively.

Since here we are interested in the intrinsic noise performances of the transimpedance amplifier, we will assume a noiseless bias source ($v_{nB} \approx 0$, obtained, for instance, resorting to a battery) so that the expression of v_n and i_n are the same in both cases. In order to evaluate the equivalent input background noise S_{iBN}, we need to evaluate the power spectrum of the term $i_n + v_n Y_D$ taking into account the correlation between the two terms. We have

$$S_{iBN} = S_{in} + S_{vn}|Y_D|^2 + S_{ic}, \tag{50}$$

MOST WIEDZY Downloaded from mostwiedzy.pl

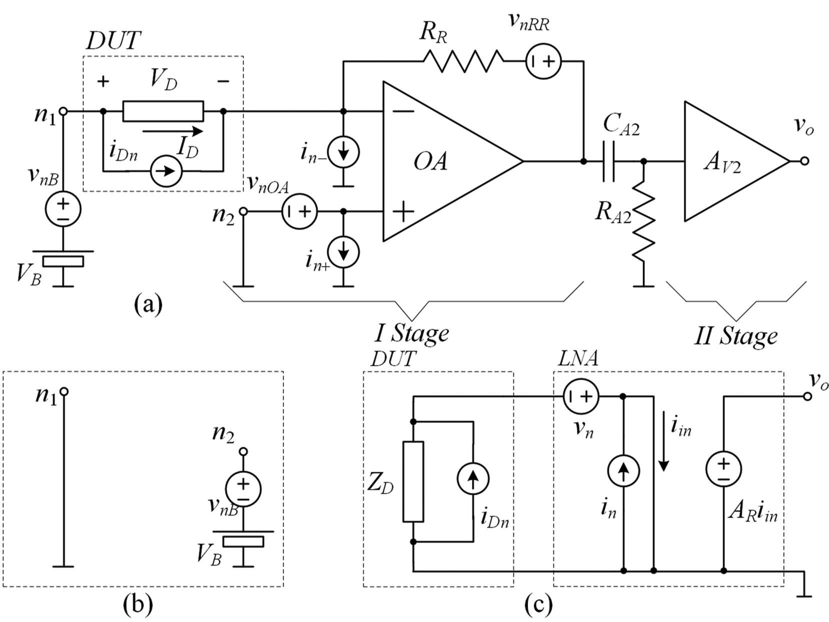

FIG. 18. Typical configuration of a transimpedance amplifier for current noise measurements on large impedance DUTs (a); an alternative bias configuration (b); and the reference circuit for the determination of the equivalent input noise sources is shown in (c).

where the term S_{ic} comes from the correlation between i_n and v_n,

$$S_{ic} = 2S_{nOA}\frac{\mathbb{R}(Y_D)}{R_R}, \tag{51}$$

and S_{in} and S_{vn} are the PSD of i_n and v_n respectively, that is (in the assumption of noiseless bias supply),

$$S_{in} = S_{in-} + \frac{S_{nOA}}{R_R^2} + \frac{S_{nRR}}{R_R^2} = S_{in-} + \frac{S_{nOA}}{R_R^2} + \frac{4kT}{R_R}, \tag{52}$$

$$S_{vn} = S_{nOA}, \tag{53}$$

where S_{in-} is the PSD of i_{n-} and S_{nRR} is the PSD of the thermal voltage noise generated by the resistance R_R.

The expressions obtained so far are useful because they clarify how each noise source contributes to the equivalent input noise sources in the equivalent circuit in Fig. 18(c), but as far as the relative weight of each source is concerned, it is more useful to have a compact expression for S_{iBN} as follows:

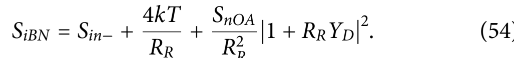

$$S_{iBN} = S_{in-} + \frac{4kT}{R_R} + \frac{S_{nOA}}{R_R^2}|1 + R_R Y_D|^2. \tag{54}$$

From Eq. (54), it is apparent that increasing R_R always results in a decrease in S_{iBN}. As we have observed earlier, the maximum value of R_R is limited by the fact that the voltage drop across R_R due to the bias current must remain within the limits allowed by the dynamic range of the OA in the transimpedance stage. Even in the case in which a low bias current could allow to employ resistances in the GΩ range, the intrinsic parasitic capacitance associated with the feedback resistance can severely limit the bandwidth of the amplifier. For instance, a 1 GΩ resistance with a parasitic capacitance in parallel of 2 pF would result in a high frequency corner below 100 Hz, and this may be unacceptable in some applications. For this reason, typical values of R_R seldom rise above a few hundred MΩ. With values of R_R above 10 MΩ, the contribution to the background noise coming from the thermal noise of R_R in Eq. (54) is below 41 fA/$\sqrt{\text{Hz}}$ at room temperature. When we take into consideration the other terms in Eq. (54), we observe that, ideally, we would like to have low levels of both equivalent input current noise and equivalent input voltage noise for the operational amplifier. Unfortunately, when we look at the best low-noise operational amplifier available on the market, current noise and voltage noise follow different trends depending on the nature of the input stage of the OA. Table I lists the performances in terms of EIVN and EICN at 1 Hz for five commonly used low-noise operational amplifiers: two amplifiers with bipolar input stages (OP27 and LT1118), one amplifier with JFET input stage (OP743), and two amplifiers with MOSFET input stages (TLC070 and TLC2201).

The devices in Table I are ordered from top to bottom for increasing EIVN. In the case of the MOSFET input OA, the reported EICN corresponds to the shot noise due to the input bias current (1 pA), and it is not specified vs frequency mostly because it is extremely difficult to perform a direct measurement at these

TABLE I. Selected noise characteristics of a few low noise operational amplifiers.

OA	Input stage	EIVN@1 Hz (nV/$\sqrt{\text{Hz}}$)	EICN@1 Hz (pA/$\sqrt{\text{Hz}}$)
LT1128	Bipolar	1.5	14
OP27	Bipolar	6.0	4.7
AD743	JFET	25	0.1
TLC2201	MOSFET	60	0.6×10^{-3} [a]
TLC070	MOSFET	90	0.6×10^{-3} [a]

[a]EICN is not specified vs frequency in the data sheet. The reported noise level corresponds to the shot noise due to the bias current (1 pA).

MOST WIEDZY Downloaded from mostwiedzy.pl

ublished under an exclusive license by AIP Publishing

extremely low levels. If we assume that the modulus of the product $|R_R Y_D|$ is not much larger that unity (save that for special cases that will be discussed in a moment, this is a reasonable assumption at low frequencies), from Eq. (54), it can be easily obtained that the contribution from S_{nOA} is relevant with respect to the contribution coming from R_R only if S_{nOA} is in the same order of the thermal voltage noise of the resistance R_R. For $R_R = 10$ MΩ, we have a thermal noise of about 400 nV/$\sqrt{\text{Hz}}$, and this means that even the largest values of EIVN in Table I can be tolerated. Our choice in the selection of the OA should therefore be based on the level of current noise. Indeed, when MOSFET input operational amplifier are used, the measurement of the background noise with $Y_D = 0$ (no DUT connected to the system) often coincides with the noise introduced by the feedback resistance. It is important to note, however, that in DUTs characterized by high impedance at very low frequencies, as the frequency increases the impedance is usually dominated by the capacitive component of the impedance and by the unavoidable parasitic capacitances that appear in parallel to the DUT simply because of its physical structure and the way in which it is connected to the amplifier and to the bias source. This means that, as the frequency increases, since $|Y_D|$ increases, the contribution from S_{nOA} may become significant. Note, however, that, as the frequency increases, the value of S_{nA} generally decreases toward a plateau in the order of 10–20 nV/$\sqrt{\text{Hz}}$ for most low noise MOSFET input operational amplifies. In order to get a sense of the weight of the contribution coming from the EIVN of the operational amplifier, we may refer to Fig. 19(b) where we report the result of SPICE simulations performed on the trans-resistance stage in Fig. 19(a) where we are assuming that the DUT is an ideal capacitor with a capacitance of 100 pF. The simulated operational amplifier is a TLC070, and the feedback resistance R_R has a value of 100 MΩ. Note that we have added a capacitance C_R that is meant to reproduce the unavoidable parasitic capacitance in parallel with R_R in actual circuits. Since we are performing simulations, we can initially assume $C_R = 0$ and we can simulate the overall S_{iBn} and the contribution from S_{nOA} in this ideal condition [curves in blue in Fig. 19(b)]. Note that S_{iBn} is obtained from the simulated PSD of the output noise divided by the ideal expected gain, with no correction for the actual frequency response of the system at higher frequencies. While this is not correct, in principle, it offers the advantage that we can discuss in terms of S_{iBn} (which is the correct one within the flat bandwidth of the amplifier) while maintaining, for the reported spectra, the same shape that would be recorded by a spectrum analyzer connected at the output of the system.

As it can be seen when looking at the blue curves in Fig. 19(b), S_{iBn} essentially coincides with the thermal current noise of the feedback resistances up to a few hundred Hz, until the rise of the contribution from S_{nOA}, because of the increase in $|Y_D|$, becomes the dominant source of noise. It must be noted that this type of behavior is seldom noticed in actual experiments. This is due to the fact that when we include the parasitic capacitance associated with the resistor R_R (2 pF in the simulation, including intrinsic parasitic capacitance and that resulting from the connection to the circuit board), the shape of the measured spectrum changes [black curves in Fig. 19(b)] and the increase in the input noise is typically hidden by the overall decrease of the measured PSD at higher frequencies. It must be noted that we could increase the value of R_R to reduce S_{iBN} (note that a larger R_R also reduces the effect of S_{nOA}). However, if the type of resistance remains the same and the circuit board remains unchanged, it is reasonable to expect that the parasitic capacitance does not change, resulting in reduction of the bandwidth by the same amount by which the PSD of the background noise is reduced.

Techniques have been developed that allow to extend the bandwidth by resorting to a number of circuit approaches intended to compensate the effect of the parasitic capacitance across R_R[123–126] that while effective may result in a significant complication of the structure of the amplifier with respect to the relatively simple design in Fig. 19(a). In addition, the limit to the largest value of R_R that can be used, given the desired maximum bias current, still remains. Another approach that can be used to reduce the background noise when the feedback resistance cannot be increased any further, either because of limitations in the bias current or because the bandwidth of the system would result too small, is to apply cross correlation techniques as it is done in the case of voltage noise measurements. For cross correlation to be possible and effective in the case of current noise measurements, we need to resort to the circuit configuration in Fig. 20(a).

Because of the virtual short at the inputs of the operational amplifiers, the DUT Z_D is biased with a constant voltage V_B. At the same time, and for the same reason, the noise signal i_D generated

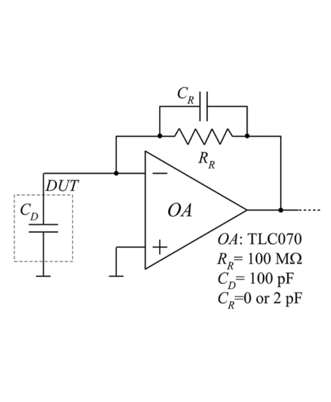

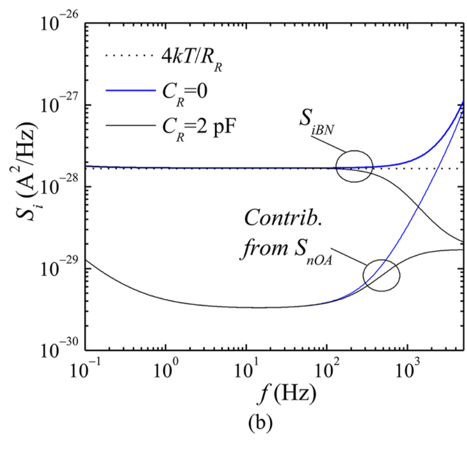

FIG. 19. Circuit for the simulation of the background noise of a transimpedance amplifier with a capacitive DUT (a); simulation results (b).

MOST WIEDZY Downloaded from mostwiedzy.pl

ublished under an exclusive license by AIP Publishing

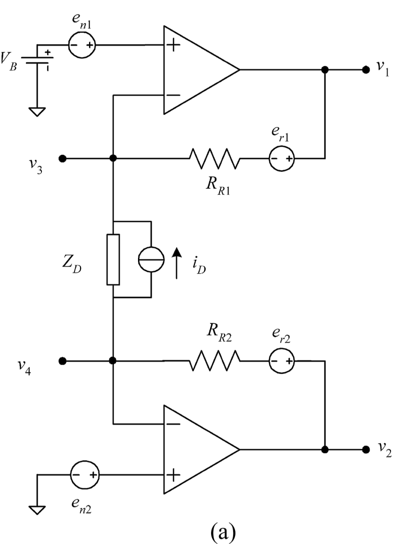

(a)

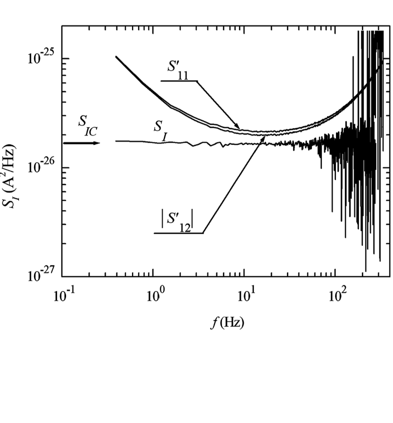

(b)

FIG. 20. Circuit configuration for the application of cross correlation approach to current noise measurements (a). Outputs v_1 and v_2 are used for the conventional two-channel approach, while outputs v_3 and v_4 are required for the advanced four channels approach.[127] The results of noise measurements in a case in which the conventional two-channel approach is not effective, but the correct result can still be obtained by resorting to the advanced approach are reported in (b). The DUT is the parallel combination of a 1 MΩ resistance with a 10 nF capacitance; R_{R1} = R_{R2} = 10 MΩ and the operational amplifiers are TLC070. (a) and (b) are reproduced with permission from Ciofi *et al.*, Rev. Sci. Instrum. **78**, 114702 (2007). Copyright 2007 AIP Publishing LLC.

by the DUT flows through both R_{R1} and R_{R2}, producing correlated signals at the outputs v_1 and v_2. It can be shown[127] that the noise generated by R_{R1} contribute to v_1 only, while the noise generated by R_{R2} contributes to v_2 only. Therefore, by performing cross correlation between the outputs v_1 and v_2, the noise contribution from the gain resistances R_{R1} and R_{R2} can be virtually eliminated. Unfortunately, each of the equivalent input noise sources e_{n1} and e_{n2} contribute to both outputs, so that their contribution is not eliminated by the cross correlation and, with respect to the simple circuit in Fig. 18(a), their contribution to the BN is essentially doubled. If the contribution from the feedback resistances is eliminated, as it should be clear from the previous discussion, the limit to the background noise becomes the noise introduced by the EIVN sources of the operational amplifiers [e_{n1} and e_{n2} in Fig. 20(a)]. In Ciofi *et al.*,[127] a method involving four channel cross correlation [involving the signals at the nodes v_1, v_2, v_3, and v_4 in Fig. 20(a)] has been developed that allows us to subtract the contribution from the EIVNs of the OAs to further reduce the background noise of the system. To appreciate the potentialities of this approach, the results of measurements performed on the parallel combination of 1 MΩ resistor with (large) 10 nF capacitance and with R_{R1} = R_{R2} = 10 MΩ are reported in Fig. 20(b). The PSD of the current noise generated by the DUT in this situation is constant and equal to the thermal noise corresponding to 1 MΩ [level S_{ID} in Fig. 20(b)]. The DUT was chosen to obtain a problematic situation in which the EIVNs of the operational amplifiers are indeed the dominant components of the BN even with respect to the noise introduced by the feedback resistances. In such a situation, two-channel cross correlation between outputs v_1 and v_2 does not provide any significant improvement to the BN [S'_{12} vs S'_{11} in Fig. 20(b)]. When the four channels correlation method is applied,[127] the correct PSD can be obtained [S_I in Fig. 20(b)]. Note that, as an alternative approach, when it is the EIVN of the OAs that sets the BN level, as in the case of DUTs with large capacitances, it is still possible to resort to a *Super* OA for the realization of the transimpedance stage in which a JFET input stage is introduced to obtain lower levels of EIVN at the cost of a slightly higher, but still tolerable, EICN.[128]

V. NOISE MEASUREMENT SET-UP

Even assuming that we have the best low-noise preamplifiers available, performing LFNM requires that a number of steps be taken in order to ensure that environmental disturbances do not couple with the measurement chain introducing artifacts that typically show up in the measured spectrum as additional noise component that has really nothing to do neither with the noise generated by the DUT nor with the BN introduced by the amplifiers and/or the bias circuit. Electro-Magnetic Interferences (EMI), either radiated or conducted, are of major concern when dealing with LFNM. It is not just that radiated and conducted interferences within the frequency band of interest can couple with different sections of the measuring chain and appear as additional component of aleatory or deterministic nature (AC power supply interferences are the typical deterministic signal) present in the spectra and, because of window leakage in spectral estimation, mask or distort the PSD we are interested in: there is a much more subtle effect that is due to radiated interferences at frequencies outside the measurement bandwidth being rectified by non-linearities in the measurement chain. What typically happens is that higher frequencies EMI coupling with the measurement systems are rectified because of non-linearities present in the circuit, resulting in a signal that often falls within the measurement bandwidth. Moreover, changes in the EMI intensity, as can be caused simply by people moving close to the measurement set up, result in a modulation of the down-converted signal, thus making even more difficult the interpretation of the measurement results.[105] The obvious countermeasure to reject the effects of EMI is to resort to careful shielding of the measurement environment. Short of resorting to a shielded room, that is not a common facility, depending on the samples and on the available instrumentation, shielding must be managed in different ways. A first distinction depends on whether the samples are available as packaged devices, or are however provided with leads for electrical connection, or need to be contacted by idle probes. As a general rule, one should try to recreate, as much as possible, a situation equivalent to that of a shielded room, with all elements of the measuring chain protected

MOST WIEDZY Downloaded from mostwiedzy.pl

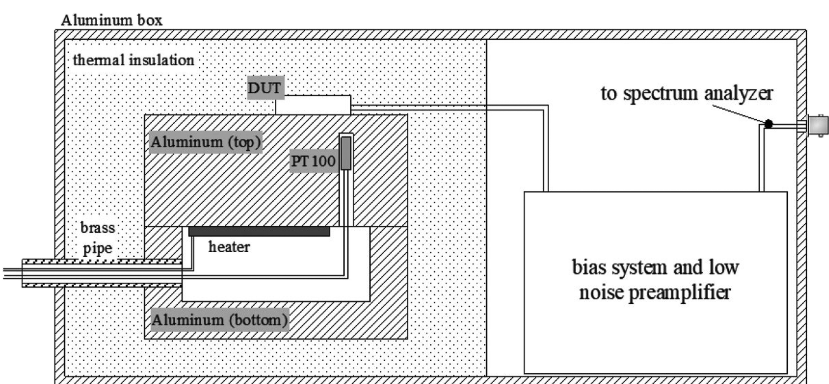

FIG. 21. Hot plate design for allowing external supply without conducted EMI. The walls of the cavity in which the heater is placed are topologically and electrically part of the external surface of the aluminum box. In this configuration, the supply cable, as well as the cables connecting to the PT100 temperature sensor, does not cross the shielding surface. Reproduced with permission from Scandurra *et al.*, Metrol. Meas. Syst. **26**, 13 (2019). Copyright 2019 Author(s), licensed under a Creative Commons Attribution 4.0 License.

by the external environment. Ideally, the bias circuit of the DUT, the DUT itself and the preamplifiers should all be enclosed in the same shielded environment with the only wiring crossing the shield being one or more BNC (or similar) connectors needed to connect the output of the amplifiers to the input of the signal acquisition system (either a benchtop spectrum analyzer or a PC controlled sampling and elaboration system). The interference-protected environment can be a metallic box with an internal volume sufficient to host the DUT, the bias system and the preamplifier stages together with the supply batteries. A common way to obtain a shielding box with quite effective shielding capabilities is to resort to a sheet of copper (1–2 mm thick) that can be cut or bended to form a box of any desired shape (in terms of length, width and depth) or to resort to commercially available aluminum boxes, with thicker walls (4 or 5 mm) that are easily available on the market. If needed, the copper (or aluminum) box can be further enclosed in another box obtained from a sheet of nickel–iron soft ferromagnetic alloy with very high permeability, commonly known as *mu-metal* that are more effective in rejecting slow changing magnetic fields than copper (or aluminum) boxes. Cobalt foil can be even more effective at low-frequency range by keeping a much lower weight.[129] There are cases, however, in which not all the subsystem and their supply can be contained in the shielded box. This can be the case, for instance, of LFNM applied to advanced metallization interconnects, where the samples have to be maintained at temperature as high as 300 °C during measurements.[39] In cases such as this, the large size of the batteries required to supply the hot plate in contact with the sample for a few hours would require a shielded box of excessive size. On the other hand, having the heather wires crossing the shielding surface to reach an external power supply generally results in an unacceptable level of conducted EMI. A possible solution to this problem is to resort to a configuration such as that reported in Fig. 21. The heater for the hot plate is placed in a cavity inside an aluminum block whose surface is topologically part of the external surface of the aluminum box acting as a shield. For this reason, the wires delivering power to the heater, together with the wires connecting to the PT100 sensor for temperature reading, never cross the shielding surface.[42]

Ideally, also the data acquisition and elaboration system should be included in the shielded environment. Optical fiber data cable could be used in this case for system configuration and to extract measurement data. This situation would indeed be essentially equivalent to using a shielded room for performing noise measurements. While this approach may appear an overkill in a number of situations, thanks to the development of efficient data elaboration libraries such as QLSA[103] and the fact that nowadays single board computers are available with sufficient computational power and reduced power consumption, it has been indeed demonstrated in Ref. 130.

When it comes to devices that have to be contacted by probes, the obvious complication lays in the fact that we need a probe station for contacting the DUT that is a part of the measurement system and needs, therefore, to be enclosed in a shielded environment. If the DUT has a limited area, however, compact solutions such as the one reported in Fig. 22 can be developed. The system in Fig. 22 is essentially a micro-probe station that can host a sample with a maximum lateral size of 5 cm with up to four probes for contacting the DUT. The bias circuits and the preamplifiers are located in the bottom section while the aluminum cover of the top section can be removed for contacting the sample and put in place during measurements for obtained effective shielding against EMI.[131]

When dealing with samples that are contacted by probes, one issue that needs to be addressed is the high level of noise that is created at the probe-pad contact. The noise generated at the point contact increases with the current supplied by the probe and can be so large that can completely mask the noise generated by the DUT.[132] Because of the dependence on the current, point contact noise shows up as a problem in voltage noise measurements on low impedance DUTs biased with a relatively large current. A typical example is noise measurements in metallic lines at wafer levels for the characterization of electromigration. A way to address this issue is to resort to four probe measurement set up together with a low noise active current source for biasing the DUT instead of the combination of a battery and a resistance in series as in Fig. 3. It can be indeed demonstrated that a very large dynamic output resistance for the current source, besides an extremely low level of current noise, is of fundamental importance for reducing the effect of contact noise.[133,134]

We have observed before that, when we are interested to frequencies below 1 Hz and high accuracy is required in the estimation of the spectra, LFNM can be quite time consuming because of the long measurement time required to accumulate enough time records to reduce the statistical error down to an acceptable level. The actual measurement process, however, can only start after the sample has been contacted and placed in the shielded environment and all

MOST WIEDZY Downloaded from mostwiedzy.pl

ublished under an exclusive license by AIP Publishing

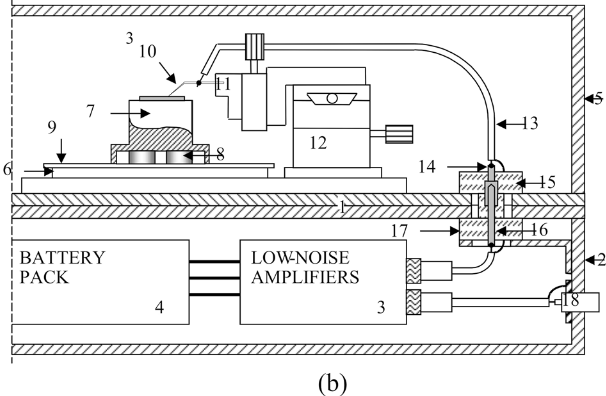

(a) (b)

FIG. 22. Microprobe for LFNM on lead-less devices (a). Bias circuits and low noise amplifiers are located in the bottom section, as shown in the cut view in (b). The system components are the two top plates (1) of two separate aluminum boxes (2 and 5) screwed together to form a supporting structure; a ferromagnetic base (6) covered by a PTFE layer for insulation (9) on top of which the sample holder (7) can slide tanks to magnets (8) for coarse positioning; a standard tungsten probe tip (10) embedded in an insulating block (11) connected to a three axis micromanipulator (12). The signal from the probe is routed toward the low noise amplifier input (3) by means of a coaxial cable (13) and an insulated pass through (14–17) that can be rapidly disconnected to reach the bottom section of system. A battery pack (4) is used to power the low noise amplifier section (3) and the output(s) is(are) sent to the spectrum analyzer via BNC connectors in the bottom section (18). Once the probes have been positioned, the upper shield is put in place with both the sample and the front-end electronics shielded from the environment. Reprinted with permission from Ciofi *et al.*, IEEE Trans. Instrum. Meas. **52**, 1533–1536 (2003). Copyright 2003 IEEE.

transients, including thermal stabilization of the measurement environment, is reached. Moreover, the fact that batteries are typically used to supply all the noise sensitive sections of the measurement chain (bias and preamplifiers), there is also the time required to recharge the battery packs. This means that, within the capabilities of a small to medium sized research laboratory, the number of measurements that can be completed in a given time can be quite limited. In order to improve the statistical significance of the results or to expand the test space (i.e., the number of bias points and the test temperature for a given DUT), some degree of automation would be beneficial. Since the typical activity in a nonindustrial research laboratory is that of understanding the noise behavior of new devices and/or searching for interpretative models of the recorded noise, each single available device is usually tested ad several bias points and, possibly, several temperatures. In this context, system automation for changing the DUT is not really useful, since several hours (in some cases several days) can be spent in order to collect noise data at all selected bias points and temperatures. As it can be easily understood, in light of the discussion in the previous sections, the design and implementation of programmable voltage or current sources to be used in LFNM system is not an easy task since the noise introduced by such systems can significantly contribute to deteriorate the background noise of the system. The noise generated by solid state voltage references and digital-analog converters can be many order of magnitudes larger than the equivalent input noise voltage of voltage preamplifiers for LFNM. As an example, the low noise AD667 DA converter by analog devices is characterized by an output noise in the order 10^{-11} V^2/Hz at 100 mHz, while the best JFET input low noise amplifiers can reach noise levels below 10^{-15} V^2/Hz at the same frequency,[110] which is more than 40 dB below. Approaches for obtaining programmable low noise voltage sources essentially fall within two main categories. In a first approach, we can start by a very low noise voltage reference, typically a battery that does not supply any current or a solid state circuit that can behave as a very low noise voltage references by avoiding Zener diodes.[135] Starting from the low noise reference, a discrete component DA converter can be built to obtain extremely low levels of noise compared to integrated DA converters.[136] While this approach can be effective, it is quite complicated in terms of the required circuitry and large number of components required. The other approach is to start from an integrated DA converter and employ a low pass filter and a low noise buffer for filtering out the excess noise in the frequency range of interest.[137–140] In this second case, the main challenge to be addressed is the fact that for a low pass filter to be effective in reducing the noise by about 40 dB at 100 mHz, the low pass filter frequency corner must be placed at about 1 mHz, thus resulting in extremely long transients whenever the voltage setting is changed. For this reason, a number of different approaches have been proposed for speeding up the transient phase. When it comes to current sources, most approaches are for obtaining low noise are based on the classical configuration that employs a low noise JFET together with a voltage source and an excess noise free resistor for setting the DC value as in Fig. 23. The DC flowing through the DUT is given by

$$I_D = \frac{V_B - V_{GS}}{R_S}. \tag{55}$$

The floating voltage source V_B can be a battery (that acts as a reference supplying a negligible current) or can even be missing (V_{GS} < 0 for the JFET in Fig. 23), in which case the supplied current depends on the DC characteristics of the employed JFET. In principle, one could replace the reference voltage V_B with a programmable low noise voltage source, thus obtaining a programmable low noise current source, but the fact the voltage source V_B must be a floating source (with no connection to ground) complicates the design, since separate battery packs should be used for the programmable

ublished under an exclusive license by AIP Publishing
MOST WIEDZY Downloaded from mostwiedzy.pl

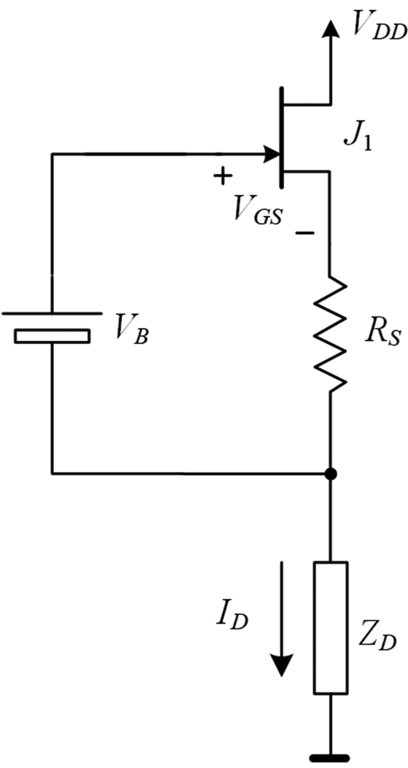

FIG. 23. Reference circuit for the realization of a low noise current source.

reference voltage and for the rest of the circuit in order to obtain different grounds. To overcome this complication, a programmable low noise current source has been proposed that is made of a set of current sources like the one in Fig. 23, all with $V_B = 0$ and whose output can be switched toward the DUT by means of a set of switches, thus essentially implementing a low noise, discrete component, current output DA converter.[141] While the approach is effective, the system is quite complex with a relatively large number of components. Thanks to the fact that LEDs coupled to integrated solar cells have become recently available, it has been possible to demonstrate that using such devices it is indeed possible to obtain a floating programmable voltage reference that can be used in place of V_B in Fig. 23, thus obtaining a quite compact programmable low noise current source.[110] Carefully designed operational amplifier based voltage to current converter can also be used to implement a programmable low noise current source.[133] Depending on the level of noise generated by the DUT, it might not be necessary to resort to dedicated low noise bias systems, and standard instrumentation already available in the laboratory can be used to build an automated low noise measurement system. This is, for instance, the case with organic FETs as discussed in Giusi *et al.*[142]

VI. LOW FREQUENCY NOISE MEASUREMENTS FOR SENSING

The basis for employing LFNM as a sensitive diagnostic tool in the investigation of the quality and reliability of electronic devices is the fact that the noise at the terminals of a DUT carries information about the detailed structure and the defects with which the charge carriers interact along their path. If the structure or the defect density changes among nominally identical devices in a production line, this can be an indication of the insurgence of a problem in the manufacturing process. For the same reason, if a device undergoes microstructural modification because of stress, this fact can be revealed by LFNM, and this is the reason why noise measurements are employed as a reliability probe. Compared with more conventional techniques, typically based on the measurements of the voltage current characteristics of an electron device, LFNM are typically characterized by higher sensitivity so that changes in the shape and amplitude of the noise spectra are observed well before they can be reliably identified by means of DC characteristics.[44] When it comes to sensor devices, we can think of them as electronic devices that undergo a change in their internal conduction mechanisms due to a change in their environment. There is therefore no surprise in the fact that their noise characteristics also change and that noise measurements, particularly low-frequency noise measurements, can reveal such changes with higher sensitivity with respect to other approaches. More importantly, a gas sensor exposed to different mixtures of agents can provide the same DC response, but since we can reasonably expect that each chemical species interacts at a different rate and, possibly, with different active sites within the sensor matrix, these differences, should result in different noise spectra. This basic idea was first tested in the mid-nineties, providing early evidence that LFNMs could indeed be used as a sensing probe and that difference in the detailed shape of the spectra could allow the discrimination among different species using a single sensor.[143,144] Since then, sensing by means of LFNM, has become known as Fluctuation Enhanced Sensing (FES). The first technical work where a FES system was proposed and mathematically and experimentally analyzed and tested as a practical tool, was published in the year 2000[145] and patents where FES plays a major role have been granted.[146–148] Over the past few years, FES has received noticeable attention, as discussed in a recent review on the subject.[95] One of the difficulties in the widespread implementation of this technique lays in the fact that minute features in the recorded spectra (typically a number of small repeated changes in the slope of the spectrum along what otherwise appears a typical flicker spectrum) have to be clearly identified, and this requires that measurement errors to be reduce to a minimum. As we have abundantly observed so far, there are many unavoidable sources of error when performing LFNM. These errors come from the very process of spectra estimation (statistical errors and systematic errors) and from the noise introduced by the instrumentation. A clear understanding of spectrum estimation process, together with the ability of designing dedicated instrumentation for obtaining the minimum background noise for a given class of sensors are of paramount importance in the further development of this quite promising technique. On the other hand, sensor optimization to enhance the sensitivity and selectivity of FES is a path that can be pursued as well.

Two-dimensional materials (2D) are highly interesting in technology and science due to their unique physical characteristics, related to repeatable structure, low dimensions, and high ratios of the active area to their volume. We can utilize their physical attributes for sensing different quantities[149] or for the realization of other electronic devices (e.g., supercapacitors,[150] high-frequency

ublished under an exclusive license by AIP Publishing

MOST WIEDZY Downloaded from mostwiedzy.pl

elements[151]). One aspect of 2D materials that is directly relevant for the subject of this paper is the fact that their inherent noise is relatively high. This can be a limitation when designing electron devices for the realization of operating circuits, but can also be an opportunity when sensors are being developed.[152] Noise phenomena, specifically low-frequency noise, are related to the quality of the 2D structures and to any physical phenomena that can interact with such structures. Hence, we must consider noise impact on 2D materials applications and investigate the mechanisms of flicker noise generation to reduce its effects in some cases (circuit design) and to exploits its potentialities in some other cases (advanced sensors design). We underline that these materials offer new opportunities for fundamentals of noise mechanisms studies because we can make the film of thickness up to a single atom layer and modify concentrations of charge transfer[153,154] so that it will be possible to associate the noise produced to the structure of the device in a more detailed way. However, since most of these materials have only recently become available, the detailed mechanisms of noise generation are still not fully recognized. Their 2D structures (Fig. 24) reveal numerous interesting properties for $1/f$ noise generation because of specific scattering mechanisms or charge trapping for different conduction mechanisms, from metallic (e.g., graphene) to semiconducting (e.g., MoS_2, WS_2, $MoSe_2$, WSe_2, ZrS_3, 1T-TaS_2) materials.

It is known that some structural imperfections, even when present within a single-atom-thick layer, result in better gas sensing properties by 2D materials since they act as adsorption and desorption centers for ambient gas molecules. These centers can be used to identify different gas molecules by means of LFNM.[155] Balandin observed in monolayer graphene devices, with an area of about tens of square μm exposed to gas, a low frequency noise component with a Lorentzian spectral density, which allows identifying a specific ambient organic vapor (e.g., ethanol, ether, and acetone). The characteristic frequencies were between dozens of Hz up to a few kHz and were identified, giving repeatable results. Noise in graphene can be relatively easily observed because of its high intensity compared with other 2D materials (e.g., MoS_2).[156,157] A graphene layer can be used as a channel in a back-gated graphene field-effect transistor (GFET). The GFET source–drain resistance is only about a few kΩ, and we can easily record its noise simply because of its relatively high intensity, compared to other more conventional electronic devices. A similar case is observed when we measure flicker noise in carbon nanotube networks exhibiting gate effect and having an even minor resistance (in the range of hundreds of ohms).[158] There is evidence that mobility fluctuations mainly generate noise in graphene because of its non-monotonical dependence on the magnetic field.[159] Noise in GFET can be measured by using a low-noise voltage amplifier and a loading resistor connected in series with the GFET that directly operates as a gas sensor.[160] The input of the voltage amplifier is connected at the drain of the FET, with the source grounded, to detect the voltage fluctuations. We determine that the observed fluctuations are generated by resistance fluctuations within the graphene structure when their power spectral density is proportional to the squared DC voltage across the sensor (voltage between drain and source terminals). When dealing with two terminal devices based on carbon materials, the conventional configuration for current noise measurements in Fig. 18 can be used.[156] Setup for operating with this type of sensors capable of measuring, at the same time, the DC response and the PSD of the noise produced by the sensor during the sensing phase have been demonstrated.[161,162]

Noise in GFETs is susceptible to ambient atmosphere and changes because of aging in a humid atmosphere. We have discovered that this detrimental effect can be reduced when graphene is situated over 2D electron gas by utilizing graphene/AlGaN/GaN structure as in radio frequency switches operating as gas sensors.[151,163] In this way, the aging rate is reduced, and the sensor exposed to laboratory air can preserve its sensing properties for months. Instead, when graphene is located over a SiO_2 dielectric layer, the graphene needs to be cleaned in a deep vacuum every 2–3 days to remove adsorbed gas molecules (H_2O, O_2^-). The aging effect of the gas sensors is observed by keeping the same noise level at different ambient atmospheres when the sensor's active surface is covered by adsorbed molecules (mainly water).

Interesting results can be observed for semiconducting 2D materials because their physical properties can be modulated by UV irradiation or metal doping.[164] Flicker noise was studied in MoS_2 samples in detail.[165] Its low-frequency noise power spectrum density depends on the ambient atmosphere. Still, it is more difficult to measure because of the higher DC resistances that require different measurement setups that increase the vulnerability to external interferences. DC resistance of some semiconducting 2D materials can reach a few hundreds of MΩ for some samples (e.g., ZrS_3).[166] 2D semiconducting materials exhibit 1/f noise generated by fluctuations in charge number according to the McWhorter model.[157]

Graphene sensors are more appropriate for utilizing low-frequency noise for gas sensing because of their lower DC resistance and observed Lorentzian characteristic in response to various gases.

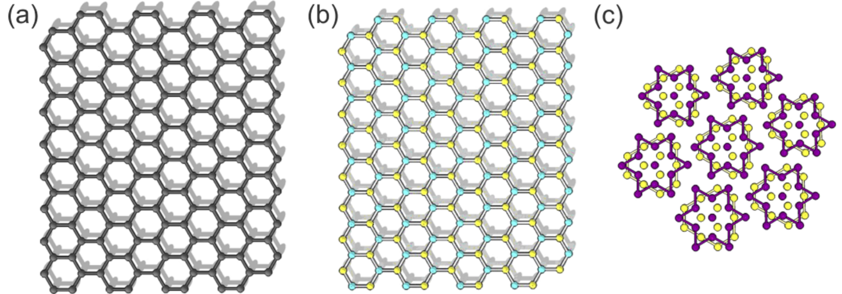

FIG. 24. Structures of 2D materials considered for sensing and flicker noise measurements: (a) graphene, (b) molybdenum disulfide (MoS_2), and (c) trigonal 1T tantalum sulfide (1T-TaS_2). The following colors were used to represent the atoms: carbon—gray, sulfur—yellow, molybdenum—aquamarine, and tantalum—purple.

ublished under an exclusive license by AIP Publishing
MOST WIEDZY Downloaded from mostwiedzy.pl

We have to apply different measurement circuits dedicated to such resistances (e.g., in magnetoresistive magnetic sensors)[167] when correlation methods are used to reduce the inherent noise of the measurement circuit. Another possible solution is to use a low-noise JFET operational amplifier as in the case of the graphene gas sensors but connected to its input and with a low-noise metallic resistor in the feedback loop. High resistances require isolation of the input of the operational amplifier by using a Teflon board to reduce possible leakage currents flowing too extensively through an ordinary printed circuit board.

Some 2D materials exhibit an exotic phenomenon called charge density waves (CDW), which induces an additional $1/f$ noise component.[152] This component can be observed even at temperatures close to room temperature in small samples locally heated by a bias current. The increased temperature begins a phase transition that induces quantum fluid of electrons observed as intensified flicker noise component. This effect can be potentially used for sensing applications. Still, it is an open question if $1/f$ noise at the transition temperatures can be modulated by the ambient atmosphere (e.g., gas or fluid). Therefore, flicker noise in the enumerated 2D materials is worth a more thorough investigation. A change of noise intensity during CDW phenomena is quite intense and can exceed one order of magnitude of noise power spectral density.[55] We underline that the CDW phenomena were observed when the 2D material was placed between the metal electrodes by inkjet printing.[168] This technology is low-cost and can be quickly introduced into practical applications.

VII. CONCLUSIONS

The field of potential application of LFNM is huge and it is expanding, since noise measurements are especially useful for the understanding of the behavior of the most advanced devices. Moreover, as we have discussed in the paper, new materials may allow expanding the application of the technique for the development of advanced sensing platforms. It is our experience that a clear understanding of all aspects of the low frequency noise measurement process can be of great help in the optimization of the measurement chain and even in the design of highly optimized measurement devices and elaboration approach for overcoming the limitation of commercially available instrumentation. For this reason, we have provided what we believe to be a simple framework for the interpretation of the mathematical process involved in the process of spectral estimation by means of DFT based spectrum analyzers. We have also discussed the problem of the measurement of the voltage and/or current noise generated by a DUT both in general terms, highlighting the most important aspects to be addressed, and by providing specific application examples and proper reference for a more detailed understanding of more advanced issues and case studies. We have also illustrated application of LFNM in the field of sensing that demonstrate the need for the development of more advanced and more sophisticated approaches for instrumentation design and data analysis. The field of LFNM related instrumentation is however a quite extensive one and cannot be covered in its entirety in a single paper. Our choice has been to select those subjects that we regard as the most fundamental ones for a clear understanding of the measurement process and in obtaining repeatable and reliable experimental results.

AUTHOR DECLARATIONS

Conflict of Interest

The authors have no conflicts to disclose.

Author Contributions

G. Scandurra: Conceptualization (lead); Investigation (equal); Methodology (equal); Supervision (lead); Validation (equal); Writing – original draft (lead); Writing – review & editing (equal). **C. Ciofi**: Conceptualization (equal); Formal analysis (lead); Investigation (equal); Methodology (equal); Validation (equal); Writing – original draft (lead); Writing – review & editing (equal). **J. Smulko**: Conceptualization (equal); Investigation (equal); Methodology (equal); Validation (equal); Writing – original draft (equal); Writing – review & editing (equal). **H. Wen**: Investigation (equal); Methodology (equal); Validation (equal); Writing – original draft (supporting); Writing – review & editing (supporting).

DATA AVAILABILITY

Data sharing is not applicable to this article as no new data were created or analyzed in this study.

REFERENCES

[1] E. J. Harris and P. O. Bishop, Nature **161**, 971 (1948).
[2] J. G. van Wijngaarden, K. M. van Vliet, and C. J. van Leeuwen, Physica **18**, 689 (1952).
[3] J. G. van Wijngaarden and K. M. van Vliet, Physica **18**, 683 (1952).
[4] J. G. van Wijngaarden and E. F. de Haan, Physica **18**, 705 (1952).
[5] T. E. Firle and H. Winston, J. Appl. Phys. **26**, 716 (1955).
[6] R. H. Kingston, J. Appl. Phys. **27**, 101 (1956).
[7] P. O. Bishop and E. J. Harris, Rev. Sci. Instrum. **21**, 366 (1950).
[8] M. D. Montgomery, J. Appl. Phys. **32**, 2408 (1961).
[9] R. H. Haitz, J. Appl. Phys. **38**, 2935 (1967).
[10] R. H. Haitz, *Fifth Annual Symposium on the Physics of Failure in Electronics* (Institute of Electrical and Electronics Engineers Inc, 1966), pp. 447–461.
[11] R. D. Baertsch, IEEE Trans. Electron Devices **ED-13**, 383 (1966).
[12] A. van der Ziel, Solid-State Electron. **9**, 123 (1966).
[13] S. Christensson and I. Lundström, Solid-State Electron. **11**, 813 (1968).
[14] S. Christensson, I. Lundström, and C. Svensson, Solid-State Electron. **11**, 797 (1968).
[15] R. A. Spaulding, Proc. IEEE **56**, 886 (1968).
[16] M. Nakahara, H. Iwasawa, and K. Yasutake, Proc. IEEE **57**, 2177 (1969).
[17] J. A. Copeland, IEEE Trans. Electron Devices **18**, 50 (1971).
[18] H.-S. Fu and C.-T. Sah, IEEE Trans. Electron Devices **19**, 273 (1972).
[19] J. W. Haslett and E. J. M. Kendall, IEEE Trans. Electron Devices **19**, 943 (1972).
[20] M. Nishida, IEEE Trans. Electron Devices **20**, 221 (1973).
[21] J. W. Haslett and E. J. M. Kendall, Proc. IEEE **61**, 1050 (1973).
[22] M. B. Das and J. M. Moore, IEEE Trans. Electron Devices **21**, 247 (1974).
[23] P. Gentil and S. Chausse, Solid-State Electron. **20**, 935 (1977).
[24] G. W. Neudeck and M. H. Kriegel, Thin Solid Films **53**, 209 (1978).
[25] F. Berz, IEEE Trans. Electron Devices **22**, 293 (1975).
[26] K. F. Knott, Solid-State Electron. **16**, 1429 (1973).
[27] M. B. Das, IEEE Trans. Electron Devices **22**, 1092 (1975).
[28] D. G. Carrigan, H. S. Fu, W. F. Stephens, A. F. Tasch, and T. F. Cheek, IEEE Trans. Electron Devices **24**, 1207 (1977).
[29] F. H. Hielscher and J. H. End, Appl. Phys. Lett. **24**, 27 (1974).
[30] K. Kandiah and F. B. Whiting, Solid-State Electron. **21**, 1079 (1978).

ublished under an exclusive license by AIP Publishing

MOST WIEDZY Downloaded from mostwiedzy.pl

[31] A. Diligenti, B. Neri, P. E. Bagnoli, A. Barsanti, and M. Rizzo, IEEE Electron Device Lett. **6**, 606 (1985).
[32] B. Neri, A. Diligenti, and P. E. Bagnoli, IEEE Trans. Electron Devices **34**, 2317 (1987).
[33] B. Neri, C. Ciofi, and V. Dattilo, IEEE Trans. Electron Devices **44**, 1454 (1997).
[34] V. Dattilo, B. Neri, and C. Ciofi, Microelectron. Reliab. **40**, 1323 (2000).
[35] C. Ciofi, I. Ciofi, S. C. Di Pascoli, and B. Neri, IEEE Trans. Instrum. Meas. **49**, 546 (2000).
[36] A. Scorzoni, B. Neri, C. Caprile, and F. Fantini, Mater. Sci. Rep. **7**, 143 (1991).
[37] G. L. Baldini, I. de Munari, A. Scorzoni, and F. Fantini, Microelectron. Reliab. **33**, 1779 (1993).
[38] Z. Çelik-Butler and M. Ye, Solid State Electron **35**, 1209 (1992).
[39] S. Beyne, L. Arnoldi, I. de Wolf, Z. Tőkei, and K. Croes, Appl. Phys. Lett. **111**, 083105 (2017).
[40] S. Beyne, O. V. Pedreira, H. Oprins, I. de Wolf, Z. Tokei, and K. Croes, IEEE Trans. Electron Devices **66**, 5278 (2019).
[41] D. M. Fleetwood, S. Beyne, R. Jiang, S. E. Zhao, P. Wang, S. Bonaldo, M. W. McCurdy, Z. Tőkei, I. DeWolf, K. Croes, E. X. Zhang, M. L. Alles, R. D. Schrimpf, R. A. Reed, and D. Linten, Appl. Phys. Lett. **114**, 203501 (2019).
[42] G. Scandurra, S. Beyne, G. Giusi, and C. Ciofi, Metrol. Meas. Syst. **26**, 13 (2019).
[43] B. Neri, P. Olivo, and B. Riccò, Appl. Phys. Lett. **51**, 2167 (1987).
[44] C. Ciofi and B. Neri, J. Phys. D: Appl. Phys. **33**, R199 (2000).
[45] A. Diligenti, B. Neri, and R. Saletti, Microelectron. Reliab. **32**, 1627 (1992).
[46] H.-S. Choi, S.-H. Hong, R.-H. Baek, K.-T. Lee, C.-Y. Kang, R. Jammy, B.-H. Lee, S.-W. Jung, and Y.-H. Jeong, IEEE Electron Device Lett. **30**, 523 (2009).
[47] S. Gerardin, A. Cester, A. Paccagnella, and G. Ghidini, Mater. Sci. Semicond. Process. **7**, 175 (2004).
[48] G. Giusi, O. Giordano, G. Scandurra, S. Calvi, G. Fortunato, M. Rapisarda, L. Mariucci, and C. Ciofi, IEEE Electron Device Lett. **36**, 390 (2015).
[49] Y. Xu, C. Liu, W. Scheideler, S. Li, W. Li, Y.-F. Lin, F. Balestra, G. Ghibaudo, and K. Tsukagoshi, IEEE Electron Device Lett. **34**, 1298 (2013).
[50] O. Marinov and M. J. Deen, *2015 International Conference on Noise and Fluctuations (ICNF)* (Institute of Electrical and Electronics Engineers Inc, 2015), pp. 1–6.
[51] L. Ke, S. B. Dolmanan, C. Vijila, S. J. Chua, Y. H. Han, and T. Mei, IEEE Trans. Electron Devices **57**, 385 (2010).
[52] Y. Xu, T. Minari, K. Tsukagoshi, J. Chroboczek, F. Balestra, and G. Ghibaudo, Solid-State Electron. **61**, 106 (2011).
[53] Y. Xu, C. Liu, H. Sun, F. Balestra, G. Ghibaudo, W. Scheideler, and Y.-Y. Noh, Org. Electron. **15**, 1738 (2014).
[54] S. Martin, A. Dodabalapur, Z. Bao, B. Crone, H. E. Katz, W. Li, A. Passner, and J. A. Rogers, J. Appl. Phys. **87**, 3381 (2000).
[55] A. Mohammadzadeh, A. Rehman, F. Kargar, S. Rumyantsev, J. M. Smulko, W. Knap, R. K. Lake, and A. A. Balandin, Appl. Phys. Lett. **118**, 223101 (2021).
[56] A. Ranjan, S. J. O'Shea, M. Bosman, N. Raghavan, and K. L. Pey, ACS Appl. Mater. Interfaces **12**, 55000 (2020).
[57] K. Lee, J. Choi, B. Kaczer, A. Grill, J. W. Lee, S. van Beek, E. Bury, J. Diaz-Fortuny, A. Chasin, J. Lee, J. Chun, D. H. Shin, J. Na, H. Cho, S. W. Lee, and G. T. Kim, Adv. Funct. Mater. **31**, 2100625 (2021).
[58] W. Liao and L. Huang, Phys. Status Solidi RRL **15**, 2100276 (2021).
[59] K. Lee, H. Ji, Y. Kim, B. Kaczer, H. Lee, J. P. Ahn, J. Choi, A. Grill, L. Panarella, Q. Smets, D. Verreck, S. van Beek, A. Chasin, D. Linten, J. Na, J. W. Lee, I. de Wolf, and G. T. Kim, Adv. Mater. Interfaces **9**, 2102488 (2022).
[60] M. Joodaki and M. Salari, Org. Electron. **59**, 230 (2018).
[61] V. K. Sangwan, M. Zhu, S. Clark, K. A. Luck, T. J. Marks, M. G. Kanatzidis, and M. C. Hersam, ACS Appl. Mater. Interfaces **11**, 14166 (2019).
[62] K. A. Luck, V. K. Sangwan, P. E. Hartnett, H. N. Arnold, M. R. Wasielewski, T. J. Marks, and M. C. Hersam, Adv. Funct. Mater. **27**, 1703805 (2017).
[63] X. Jia and L. He, AIP Adv. **11**, 045206 (2021).
[64] A. Ng, Z. Ren, C. Liu, A. B. Djurišić, R. Zhu, D. L. Phillips, and C. Surya, Proc. SPIE **10919**, 1091905 (2019).
[65] G. Landi, C. Barone, C. Mauro, H. C. Neitzert, and S. Pagano, AIP Conf. Proc. **2082**, 020001 (2019).
[66] G. Landi, C. Barone, C. Mauro, S. Pagano, and H. C. Neitzert, in *2018 IEEE International Reliability Physics Symposium (IRPS)* (IEEE, 2018), pp. 6C.3-1–6C.3-6.
[67] A. Kumar, U. Bansode, S. Ogale, and A. Rahman, Nanotechnology **31**, 365403 (2020).
[68] M.-K. Joo, Y. Yun, H. Ji, and D. Suh, Nanotechnology **30**, 035206 (2018).
[69] M. T. Mbumba, D. M. Malouangou, J. M. Tsiba, L. Bai, Y. Yang, and M. Guli, Solar Energy **230**, 954 (2021).
[70] X.-R. Nie, M. Zhang, H. Zhu, L. Chen, Q.-Q. Sun, and D. W. Zhang, IEEE Electron Device Lett. **39**, 739 (2018).
[71] C. Wulles, Q. Rafhay, T. Desrues, A. Kaminski, and C. Theodorou, Solid-State Electron. **194**, 108327 (2022).
[72] K. Achtenberg, J. Mikołajczyk, C. Ciofi, G. Scandurra, K. Michalczewski, and Z. Bielecki, Measurement **183**, 109867 (2021).
[73] K. Achtenberg, J. Mikołajczyk, C. Ciofi, G. Scandurra, and Z. Bielecki, Measurement **190**, 110657 (2022).
[74] N. Dyakonova, S. A. Karandashev, M. E. Levinshtein, B. A. Matveev, and M. A. Remennyi, Infrared Phys. Technol. **111**, 103460 (2020).
[75] N. Dyakonova, S. A. Karandashev, M. E. Levinshtein, B. A. Matveev, and M. A. Remennyi, Semicond. Sci. Technol. **35**, 075010 (2020).
[76] N. Dyakonova, S. A. Karandashev, M. E. Levinshtein, B. A. Matveev, M. A. Remennyi, and A. A. Usikova, Infrared Phys. Technol. **117**, 103867 (2021).
[77] L. Zhu, J. Huang, Z. Xie, Z. Deng, L. Chen, C. Lin, and B. Chen, IEEE Trans. Electron Devices **67**, 547 (2020).
[78] L. Zhu, Z. Deng, J. Huang, H. Guo, L. Chen, C. Lin, and B. Chen, Opt. Express **28**, 23660 (2020).
[79] V. Dhyani, G. Ahmad, N. Kumar, and S. Das, IEEE Trans. Electron Devices **67**, 558 (2020).
[80] N. Zhang, A. H. Jones, Z. Deng, and B. Chen, Opt. Express **28**, 11682 (2020).
[81] C.-K. Wang, Y.-Z. Chiou, and Y.-L. Huang, IEEE Sens. J. **21**, 23995 (2021).
[82] N.A.M. Tran *et al.*, Nanotechnology **32**, 045502 (2020).
[83] G. Jung, W. Shin, S. Hong, Y. Jeong, J. Park, D. Kim, J.-H. Bae, B.-G. Park, and J.-H. Lee, Sens. Actuators, B **335**, 129661 (2021).
[84] K. Czuba, Ł. Ciura, I. Sankowska, E. Papis-Polakowska, and A. Jasik, Sensors **21**, 7005 (2021).
[85] S. Liang *et al.*, Nanotechnology and Precision Engineering **3**, 9 (2020).
[86] T. Ciuk, Ł. Ciura, P. P. Michałowski, J. Jagiełło, A. Dobrowolski, K. Piętak, D. Kalita, M. Wzorek, R. Budzich, D. Czołak, and A. Kolek, Physica E **142**, 115264 (2022).
[87] P. Bhattacharyya, IEEE Sens. J. **21**, 10231 (2021).
[88] W. Shin, S. Hong, Y. Jeong, G. Jung, B.-G. Park, and J.-H. Lee, IEEE Trans. Electron Devices **69**, 2604 (2022).
[89] D. Kim, W. Shin, S. Hong, Y. Jeong, G. Jung, J. Park, and J.-H. Lee, IEEE Sens. J. **22**, 6311 (2022).
[90] J. Nah, F. K. Perkins, E. H. Lock, A. Nath, A. Boyd, R. L. Myers-Ward, D. K. Gaskill, M. Osofsky, and M. V. Rao, Sensors **22**, 1183 (2022).
[91] W. Shin, Y. Jeong, S. Hong, G. Jung, J. Park, D. Kim, B.-G. Park, and J.-H. Lee, Sens. Actuators, B **367**, 132052 (2022).
[92] W. Shin, D. Kwon, M. Ryu, J. Kwon, S. Hong, Y. Jeong, G. Jung, J. Park, D. Kim, and J.-H. Lee, Sens. Actuators, B **344**, 130148 (2021).
[93] A. Polley, A. V. Ravichandran, V. S. Kumar, A. Venugopal, L. Cheng, A. T. Lucero, J. Kim, L. Colombo, and R. R. Doering, IEEE Sens. J. **21**, 25675 (2021).
[94] A. Rehman, A. Krajewska, B. Stonio, K. Pavlov, G. Cywinski, D. Lioubtchenko, W. Knap, S. Rumyantsev, and J. M. Smulko, Appl. Phys. Lett. **118**, 242102 (2021).
[95] G. Scandurra, J. M. Smulko, and L. B. Kish, Appl. Sci. **10**, 5818 (2020).
[96] A. der Ziel, *Noise in Solid State Devices and Circuits* (Wiley-Interscience, 1986).
[97] A. Papoulis and S. U. Pillai, *Probability, Random Variables, and Stochastic Processes* (Tata McGraw-Hill Education, 2002).
[98] W. B. Davenport, R. A. Johnson, and D. Middleton, J. Appl. Phys. **23**, 377 (1952).
[99] R. R. Bennett and A. S. Fulton, J. Appl. Phys. **22**, 1187 (1951).
[100] P. Welch, IEEE Trans. Audio Electroacoust. **15**, 70 (1967).

MOST WIEDZY Downloaded from mostwiedzy.pl

[101] A. H. Nuttail, "Spectral estimation by means of overlapped fast Fourier transform processing of windowed data," Report No. 4169 (Naval Underwater Systems Center, New London, CT, 1971).
[102] G. Giusi, G. Scandurra, and C. Ciofi, Fluctuation Noise Lett. **12**, 1350007 (2013).
[103] C. Ciofi, G. Scandurra, and G. Giusi, Fluctuation Noise Lett. **18**, 1940004 (2019).
[104] Z. Çelik-Butler, W. Yang, H. H. Hoang, and W. R. Hunter, Solid State Electronics **34**, 185 (1991).
[105] C. Ciofi, G. Giusi, G. Scandurra, and B. Neri, Fluctuation Noise Lett. **04**, L385 (2004).
[106] G. Giusi, F. Crupi, C. Pace, and P. Magnone, IEEE Trans. Circuits Syst. **56**, 97 (2009).
[107] H. A. Haus, W. R. Atkinson, G. M. Branch, W. B. Davenport, W. H. Fonger, W. A. Harris, S. W. Harrison, W. W. Mcleod, E. K. Stodola, and T. E. Talpey, Proc. IRE **48**, 69 (1960).
[108] G. Cannatà, G. Scandurra, and C. Ciofi, Rev. Sci. Instrum. **80**, 114702 (2009).
[109] Analog Devices, Inc., https://Www.Analog.Com/Media/En/Technical-Documentation/Data-Sheets/SSM2220.Pdf, 2013.
[110] G. Scandurra, G. Cannatà, G. Giusi, and C. Ciofi, Rev. Sci. Instrum. **85**, 125109 (2014).
[111] C. Ciofi, M. de Marinis, and B. Neri, IEEE Trans. Instrum. Meas. **46**, 789–793 (1997).
[112] K. Achtenberg, J. Mikołajczyk, and Z. Bielecki, Metrol. Meas. Syst. **27**, 531 (2020).
[113] B. Neri, B. Pellegrini, and R. Saletti, IEEE Trans. Instrum. Meas. **40**, 2 (1991).
[114] G. Scandurra, G. Cannat, and C. Ciofi, AIP Adv. **1**, 022144 (2011).
[115] G. Scandurra, G. Cannata, G. Giusi, and C. Ciofi, in *2013 22nd International Conference on Noise and Fluctuations, ICNF 2013* (Institute of Electrical and Electronics Engineers Inc., 2013).
[116] G. Scandurra, K. Achtenberg, Z. Bielecki, J. Mikołajczyk, and C. Ciofi, Electronics **11**, 2011 (2022).
[117] A. Hassibi, R. Navid, R. W. Dutton, and T. H. Lee, J. Appl. Phys. **96**, 1074 (2004).
[118] E. Rubiola, *EFTF 2008 - 22nd European Frequency and Time* (Forum European Frequency and Time Forum EFTF, 2008).
[119] F. Crupi, G. Giusi, C. Ciofi, and C. Pace, IEEE Trans. Instrum. Meas. **55**, 1143 (2006).
[120] M. Sampietro, L. Fasoli, and G. Ferrari, Rev. Sci. Instrum. **70**, 2520 (1999).
[121] G. Scandurra and C. Ciofi, in *2012 IEEE I2MTC - International Instrumentation and Measurement Technology Conference* (IEEE, 2012), pp. 1524–1528.
[122] G. Scandurra, G. Giusi, and C. Ciofi, IEEE Trans. Instrum. Meas. **62**, 1145 (2013).
[123] G. Ferrari and M. Sampietro, Rev. Sci. Instrum. **78**, 094703 (2007).
[124] C. Ciofi, F. Crupi, C. Pace, and G. Scandurra, IEEE Trans. Instrum. Meas. **55**, 814 (2006).
[125] B. Su, X. Yang, H. Cui, and D. R. Jones, Rev. Sci. Instrum. **93**, 043004 (2022).
[126] G. Giusi, G. Cannatà, G. Scandurra, and C. Ciofi, Int. J. Circuit Theory Appl. **43**, 1455 (2015).
[127] C. Ciofi, G. Scandurra, R. Merlino, G. Cannatà, and G. Giusi, Rev. Sci. Instrum. **78**, 114702 (2007).
[128] M. Carminati, G. Ferrari, M. Sampietro, A. P. Ivanov, and T. Albrecht, in *2012 19th IEEE International Conference on Electronics, Circuits, and Systems (ICECS 2012)* (IEEE, 2012), pp. 817–820.
[129] EMR Shielding Solutions, https://Www.Emrss.Com/Products/Magnetic-Shielding-Mcf5, 2022.
[130] E. Cardillo, G. Scandurra, G. Giusi, and C. Ciofi, Sensors **21**, 4307 (2021).
[131] C. Ciofi, F. Crupi, C. Pace, and G. Scandurra, IEEE Trans. Instrum. Meas. **52**, 1533 (2003).
[132] A. M. Yassine, T. M. Clien, and B. A. Beitman, IEEE Electron Device Lett. **12**, 200 (1991).
[133] J.-M. Routoure, S. Wu, C. Barone, L. Mechin, and B. Guillet, IEEE Trans. Instrum. Meas. **69**, 194 (2020).
[134] C. Ciofi, M. de Marinis, and B. Neri, Microelectron. Reliab. **36**, 1851 (1996).
[135] C. Ciofi, G. Scandurra, and G. Cannata, IEEE Trans. Instrum. Meas. **59**, 2724 (2010).
[136] L. Baracchino, G. Basso, C. Ciofi, and B. Neri, IEEE Trans. Instrum. Meas. **46**, 1256 (1997).
[137] V. E. Ivanov and E. U. Chye, J. Phys.: Conf. Ser. **1015**, 052011 (2018).
[138] K. Achtenberg, J. Mikołajczyk, C. Ciofi, G. Scandurra, and Z. Bielecki, Electronics **9**, 1245 (2020).
[139] C. Pace, C. Ciofi, and F. Crupi, IEEE Trans. Instrum. Meas. **52**, 1251 (2003).
[140] G. Scandurra, G. Giusi, and C. Ciofi, Rev. Sci. Instrum. **85**, 044702 (2014).
[141] D. Talukdar, R. K. Chakraborty, S. Bose, and K. K. Bardhan, Rev. Sci. Instrum. **82**, 013906 (2011).
[142] G. Giusi, O. Giordano, G. Scandurra, M. Rapisarda, S. Calvi, and C. Ciofi, Rev. Sci. Instrum. **87**, 044702 (2016).
[143] P. Bruschi, A. Nannini, and B. Neri, Sens. Actuators, B **25**, 429 (1995).
[144] P. Bruschi, F. Cacialli, A. Nannini, and B. Neri, Sens. Actuators, B **19**, 421 (1994).
[145] L. B. Kish, R. Vajtai, and C. G. Granqvist, Sens. Actuators, B **71**, 55 (2000).
[146] S. Janusz, K. L. B, and S. Gabor, "System and method for gas recognition by analysis of bispectrum functions," U.S. Patent 7,680,607 (16 March 2010).
[147] K. L. B, G. Claes-Goeran, and V. Robert, "Sampling and hold technique for analyzing chemical compositions, especially gas sensing, involves heating sensors before allowing them to cool and evaluating noise fluctuation spectrum," Patent No. SE 515,249 C2 (2 July 2001).
[148] K. L. B, G. Claes-Goeran, and S. Jan, "Detection of chemicals based on resistance fluctuation-spectroscopy," Patent No. SE 9803019 D0 (7 September 1998).
[149] C. Anichini, W. Czepa, D. Pakulski, A. Aliprandi, A. Ciesielski, and P. Samorì, Chem. Soc. Rev. **47**, 4860 (2018).
[150] Poonam, K. Sharma, A. Arora, and S. K. Tripathi, J. Energy Storage **21**, 801 (2019).
[151] Y. Yashchyshyn, P. Bajurko, J. Sobolewski, P. Sai, A. Przewłoka, A. Krajewska, P. Prystawko, M. Dub, W. Knap, S. Rumyantsev, and G. Cywiński, Micromachines **12**, 1343 (2021).
[152] A. A. Balandin and S. Rumyantsev, "Low-Frequency Noise in Low-Dimensional van der Waals Materials," arXiv.1908.06204.
[153] A. C. Ferrari, J. C. Meyer, V. Scardaci, C. Casiraghi, M. Lazzeri, F. Mauri, S. Piscanec, D. Jiang, K. S. Novoselov, S. Roth, and A. K. Geim, Phys. Rev. Lett. **97**, 187401 (2006).
[154] C. N. R. Rao and R. Voggu, Mater. Today **13**, 34 (2010).
[155] A. A. Balandin, Nat. Nanotechnol. **8**, 549 (2013).
[156] J. Na, M.-K. Joo, M. Shin, J. Huh, J.-S. Kim, M. Piao, J.-E. Jin, H.-K. Jang, H. J. Choi, J. H. Shim, and G.-T. Kim, Nanoscale **6**, 433 (2014).
[157] J. Renteria, R. Samnakay, S. L. Rumyantsev, C. Jiang, P. Goli, M. S. Shur, and A. A. Balandin, Appl. Phys. Lett. **104**, 153104 (2014).
[158] K. Drozdowska, A. Rehman, A. Krajewska, D. v. Lioubtchenko, K. Pavłov, S. Rumyantsev, J. Smulko, and G. Cywiński, Sens. Actuators, B **352**, 131069 (2022).
[159] A. Rehman, J. A. Delgado Notario, J. Salvador Sanchez, Y. M. Meziani, G. Cywiński, W. Knap, A. A. Balandin, M. Levinshtein, and S. Rumyantsev, Nanoscale **14**, 7242 (2022).
[160] B. Ayhan, C. Kwan, J. Zhou, L. B. Kish, K. D. Benkstein, P. H. Rogers, and S. Semancik, Sens. Actuators, B **188**, 651 (2013).
[161] A. Kwiatkowski, K. Drozdowska, and J. Smulko, Rev. Sci. Instrum. **92**, 074102 (2021).
[162] J. Smulko, T. Chludziński, T. Majchrzak, A. Kwiatkowski, S. Borys, A. Lisset Jaimes-Mogollón, C. Manuel Durán-Acevedo, O. Geovanny Perez-Ortiz, and R. Ionescu, Measurement **190**, 110733 (2022).
[163] A. Bag, D.-B. Moon, K.-H. Park, C.-Y. Cho, and N.-E. Lee, Sens. Actuators, B **296**, 126684 (2019).
[164] T. Pham, G. Li, E. Bekyarova, M. E. Itkis, and A. Mulchandani, ACS Nano **13**, 3196 (2019).

ublished under an exclusive license by AIP Publishing

MOST WIEDZY Downloaded from mostwiedzy.pl

[165]G. Liu, S. L. Rumyantsev, C. Jiang, M. S. Shur, and A. A. Balandin, IEEE Electron Device Lett. **36**, 1202 (2015).
[166]A. Patel, C. Limberkar, K. Patel, S. Bhakhar, K. D. Patel, G. K. Solanki, and V. M. Pathak, Sens. Actuators, A **331**, 112969 (2021).
[167]N. A. Stutzke, S. E. Russek, D. P. Pappas, and M. Tondra, J. Appl. Phys. **97**, 10Q107 (2005).
[168]S. Baraghani, Z. Barani, Y. Ghafouri, A. Mohammadzadeh, T. T. Salguero, F. Kargar, and A. A. Balandin, ACS Nano **16**, 6325 (2022).

MOST WIEDZY Downloaded from mostwiedzy.pl

ublished under an exclusive license by AIP Publishing